Scientific Excellence • Resource Protection & Conservation • Benefits for Canadians
Excellence scientifique • Protection et conservation des ressources • Bénéfices aux Canadiens

Statistical Estimates and Dynamical Interpretations of Bottom Pressure Variations Over the Labrador/Newfoundland Shelf

D.G. Wright, D.A. Greenberg, and J.F. Middleton

Physical and Chemical Sciences Branch
Scotia-Fundy Region
Department of Fisheries and Oceans

Bedford Institute of Oceanography
P.O. Box 1006
Dartmouth, Nova Scotia
Canada B2Y 4A2

1991

Canadian Technical Report of Hydrography and Ocean Sciences No. 131

Canadian Technical Report of Hydrography and Ocean Sciences

Technical reports contain scientific and technical information that contributes to existing knowledge but which is not normally appropriate for primary literature. The subject matter is related generally to programs and interests of the Ocean Science and Surveys (OSS) sector of the Department of Fisheries and Oceans.

Technical reports may be cited as full publications. The correct citation appears above the abstract of each report. Each report is abstracted in *Aquatic Sciences and Fisheries Abstracts* and indexed in the Department's annual index to scientific and technical publications.

Technical reports are produced regionally but are numbered nationally. Requests for individual reports will be filled by the issuing establishment listed on the front cover and title page. Out of stock reports will be supplied for a fee by commercial agents.

Regional and headquarters establishments of Ocean Science and Surveys ceased publication of their various report series as of December 1981. A complete listing of these publications is published in the *Canadian Journal of Fisheries and Aquatic Sciences*, Volume 39: Index to Publications 1982. The current series, which begins with report number 1, was initiated in January 1982.

Rapport technique canadien sur l'hydrographie et les sciences océaniques

Les rapports techniques contiennent des renseignements scientifiques et techniques qui constituent une contribution aux connaissances actuelles, mais qui ne sont pas normalement appropriés pour la publication dans un journal scientifique. Le sujet est généralement lié aux programmes et intérêts du service des Sciences et levés océaniques (SLO) du ministère des Pêches et des Océans.

Les rapports techniques peuvent être cités comme des publications complètes. Le titre exact paraît au-dessus du résumé de chaque rapport. Les rapports techniques sont résumés dans la revue *Résumés des sciences aquatiques et halieutiques*, et ils sont classés dans l'index annuel des publications scientifiques et techniques du Ministère.

Les rapports techniques sont produits à l'échelon régional, mais numérotés à l'échelon national. Les demandes de rapports seront satisfaites par l'établissement auteur dont le nom figure sur la couverture et la page du titre. Les rapports épuisés seront fournis contre rétribution par des agents commerciaux.

Les établissements des Sciences et levés océaniques dans les régions et à l'administration centrale ont cessé de publier leurs diverses séries de rapports en décembre 1981. Une liste complète de ces publications figure dans le volume 39, Index des publications 1982 du *Journal canadien des sciences halieutiques et aquatiques*. La série actuelle a commencé avec la publication du rapport numéro 1 en janvier 1982.

91-05069/

Canadian Technical Report of
Hydrography and Ocean Sciences No. 131

April 1991

STATISTICAL ESTIMATES AND DYNAMICAL INTERPRETATIONS OF BOTTOM PRESSURE VARIATIONS OVER THE LABRADOR/NEWFOUNDLAND SHELF

by

D.G. Wright, D.A. Greenberg
and J.F. Middleton[1]

Physical and Chemical Sciences Branch
Scotia-Fundy Region
Department of Fisheries and Oceans

Bedford Institute of Oceanography
P.O. Box 1006
Dartmouth, Nova Scotia
Canada B2Y 4A2

[1]School of Mathematics
University of New South Wales
Kensington, N.S.W.
Australia 2033

ACKNOWLEDGMENTS

We would like to thank everyone who assisted with the deployment and recovery of instrumentation, most notably John Lazier and Charles Tang. We also thank Gary Bugden and Ken Drinkwater for their helpful comments on the manuscript, Brian Petrie for his assistance through his role as PERD project manager, and Meg Burhoe for typing the manuscript. This work was partially funded by the Canadian Federal Panel on Energy Research and Development.

Minister of Supply and Services 1991

Cat. No. Fs 97–18/131 E ISSN-0711–6764

Correct citation for this publication:

D.G. Wright, D.A. Greenberg, and J.F. Middleton. 1991. Statistical estimates and dynamical interpretations of bottom pressure variations over the Labrador/Newfoundland Shelf. Can. Tech. Rep. Hydrogr. Ocean Sci. No. 131: v+ 60 pp.

TABLE OF CONTENTS

		Page
Acknowledgements		ii
Abstract		iv
1.	Introduction	1
2.	Data Set	3
3.	A Cursory Description of the Data	4
4.	Statistical Models/Separation of Remotely and Locally Forced Motions	5
5.	Regression Results	7
6.	Discussion and Conclusions	11
References		14
Appendix: The Numerical Model		17
Tables		19
Figures		26

ABSTRACT

D.G. Wright, D.A. Greenberg, and J.F. Middleton. 1991. Statistical estimates and dynamical interpretations of bottom pressure variations over the Labrador/Newfoundland Shelf. Can. Tech. Rep. Hydrogr. Ocean Sci. No. 131: v+ 60 pp.

Results from an array of 17 pressure gauges covering the region from Nain Bank to the Grand Bank are presented and discussed. Complex empirical orthogonal functions are used to demonstrate the large scale nature of the sub-tidal pressure changes in this region: 80% or more of the total variance over the 17 records is contained in the first two empirical modes. Separate analysis of the four gauges across Nain Bank alone shows that after an estimate of the "offshore" influence (approximated by the pressure near the shelf break where pressure variations associated with coastally trapped wave energy is expected to be small) is removed, 95% of the remaining energy in the four gauges is contained in the first empirical mode. This empirical mode is taken to represent the coastally trapped wave energy entering the measurement domain across Nain Bank.

Multiple regression in the frequency domain is used to relate the observed pressure variations to coastally trapped waves propagating by Nain Bank, the "offshore" influence and local wind stress. The coastally trapped wave amplitude is found to decrease much more rapidly along the shelf than it would on a smooth shelf where it is dissipated by frictional stresses alone. This result supports suggestions from numerical and analytical studies that wave energy is scattered by the rugged shelf topography. Pressure variations associated with the "offshore" influence are found to be substantial at all sites. The spatial structure corresponding to this influence is a nearly uniform rise and fall of pressure over the whole array, with some suggestion of phase propagation and increasing amplitude in the direction of coastally trapped wave propagation. The response to cross-shelf wind stress is relatively small compared to the other forcing effects. The response to alongshelf wind stress increases in amplitude southward with higher pressure associated with southward stress, at least qualitatively consistent with expectations.

Our results are qualitatively consistent with simple theoretical models, but it is clear that the rugged topography of the region does play an important role. In particular, the topography appears to scatter energy into smaller scale features which impedes the signal transfer along the shelf, and complicates the interpretation of results.

RÉSUMÉ

Wright, D.G., D.A. Greenberg, and J.F. Middleton. 1991. Statistical estimates and dynamical interpretations of bottom pressure variations over the Labrador/Newfoundland Shelf. Can. Tech. Rep. Hydrogr. Ocean Sci. No. 131: v+ 60 pp.

Les résultats d'un réseau de 17 jauges de pression couvrant la région allant du banc Nain au Grand banc sont présentés et analysés. Des fonctions orthogonales empiriques complexes sont utilisées pour établir la nature à grande échelle des variations de pression infralittorales dans cette région: 80 % ou plus de la variance totale des 17 enregistrements se trouve dans les deux premiers modes empiriques. La seule analyse séparée des quatre jauges du banc Nain montre qu'une fois éliminé l'effet estimé "du large" (mesuré par la pression près de l'accore du plateau continental où les variations de pression associées à l'énergie des vagues piégées par la côte devraient être faibles), 95 % de l'énergie résiduele dans les quatre jauges se trouve dans le premier mode empirique. Ce mode empirique représenterait l'énertie des vagues piégées par la côte qui entre dans le domaine de mesure sur le banc Nain.

Une courbe de régression multiple est établie dans le domaine fréquenciel pour mettre en relation les variations de pression observées avec les vagure piégées par la côte qui se propagent sur le banc Nain, l'effet "du large" et la force exercée localement par le vent. L'amplitude des vagues piégées par la côte diminue beaucoup plus rapidement parallèlement au plateau qu'elle ne le ferait sur un plateau uniforme sous l'effet des seules contraintes de frottement. Ce résultat corroborent les conclusions d'études numériques et analytiques selon lesquelles l'énergie des vagues est dissipée par le relief accidenté du plateau. Les variations de pression associées à l'effet "du large" sont importantes partour. La structure spatiale correspondant à cet effet est une montée et une chute de pression presque uniformes dans tout le réseau, avec des signes de propagation de phase et d'amplitude croissante dans la direction de propagation des vagues piégées par la côte. La réponse à la force exercée par le vent en travers du plateau est relativement faible par raport aux autres forces. La réponse à la force exercée par le vent parallèlement au plateau croît en amplitude vers le sud en fonction de la pression plus élevée associée à la force exercée vers le sud, comme prévu du moins qualitativement.

Nos résultats sont qualitativement en accord avec les modèles théoriques simples, mais il est clair que le relief accidenté de la région joue un rôle important. Par exemple, le relief semble dissiper l'énergie dans les petits obstacles, ce qui gêne la propagation des signaux parallèlement au plateau et complique l'interprétation des résultats.

1. INTRODUCTION

Over the last few years there have been several papers and reports published in which subsurface pressure variations have been examined in an attempt to understand the response of the Labrador Shelf to meteorological forcing. Garrett *et al.* (1985) examined the relationship between sea-level data from Nain, Labrador (Fig. 1) and local atmospheric pressure and geostrophic wind and wind stress. At very low frequencies (periods greater than two months) sea level variations were dominated by the isostatic response to atmospheric pressure changes and the response to wind stress was found to be consistent with the results of Thompson *et al.* (1986) obtained from an analysis of a longer time series of monthly means. At higher frequencies (periods of 2 to 10 days) Garrett *et al.* (1985) found that while sea level variations could be statistically related to the wind stress and atmospheric pressure, the statistically determined relations were not consistent with the predictions of simple dynamical models.

Anderson (1986) examined sea level (and current) variations in the Avalon Channel (offshore of St. John's) in terms of buoyancy forcing, atmospheric pressure and wind stress. He found that sea level responds roughly isostatically to atmospheric pressure variations and 180° out of phase with longshore wind stress (positive for wind directed toward 330° T) at periods greater than 2 days. The latter result was difficult to reconcile with predictions of simple dynamical models. Anderson suggested that this rapid response to wind forcing indicates that the sea level response is due to continental shelf waves originating at or south of the northern edge of the Grand Bank. However, he also noted that for periods less than 10 days there was an unexplained, statistically significant lag of sea level behind the purely isostatic response, and the magnitude of his model-predicted response to alongshore stress was roughly 4.5 times smaller than that observed.

Thus, in two detailed studies of the response of coastal sea level over the Labrador/Newfoundland Shelf to meteorological forcing, it was found that statistically determined results showed substantial deviations from expectations based on simple dynamical models. Wright *et al.* (1987) later showed that the Nain sea level record is consistent with dynamical models if account is taken of coastally trapped waves which are generated by water being pumped in and out through Hudson Strait as Hudson Bay adjusts to atmospheric pressure variations. This explained the strange results obtained by Garrett *et al.* (1985). The results of Anderson (1986) have not yet been reconciled with dynamical expectations. Further, it is not clear whether or not waves originating at Hudson Strait could have any effect on sea level at St. John's some 1500 km away along a very rugged shelf. Previous theoretical studies (eg. Wang, 1980; Wilkin and Chapman, 1987; Webster, 1987; Middleton and Wright, 1988) indicate that there will be some scattering of the coherent wave field but these studies have been based on highly idealized barotropic models.

To illustrate the influence of realistic, rugged bottom topography on the propagation of coastally trapped waves (CTW's) over the Labrador/Newfoundland Shelf, a barotropic primitive equation numerical model (Appendix A)

was forced by periodic sea-level variations specified at the northern (upstream) boundary with cross-shelf structure as illustrated in Fig. 2. Figures 3a, b, c correspond to heavily smoothed topography in which actual depths less than 600 m were set equal to 200 m and the resulting topography was smoothed as in Anderson and Corry (1985). Figures 3d, e, f correspond to the more realistic case in which the actual topography was simply smoothed as in Anderson and Corry (1985). The forcing period in each case was 4 days. In the former case, the forcing results in wave propagation down the shelf which is clearly dominated by the first shelf wave mode with an average alongshelf phase speed of about 17 ms^{-1} and a decrease in sea level variations by about 25% over approximately 1500 km between Nain and St. John's. The latter (and more realistic topography) case is distinctly different. In particular, there are very large cross-shelf phase variations, alongshelf phase speed is not well-defined, and the amplitude of the sea level variations is irregular and clearly decreases more rapidly with distance down the shelf than it did with the heavily smoothed topography. These results are based on a model with rather poor horizontal resolution (one-fifth of a degree in latitude and one-third of a degree in longitude) but runs with doubled resolution show the same qualitative features (though quantitative details are modified).

Unfortunately there are intrinsic questions about the validity of predictions based on barotropic models in areas of rugged bottom topography. In particular, sufficiently strong density stratification may prevent backscattering of energy through the elimination of the short waves present in barotropic models, which carry energy in the backward direction along the shelf (Huthnance, 1978; Chapman, 1983; Middleton and Wright, 1989).

In a theoretical study of mode scattering Brink (1986) includes the influence of stratification. However, his work is relevant only to the case of small-scale topographic variations and it begins with the long-wave approximation so the possibility of scattering into small-scale waves, which can propagate energy backwards along the shelf, is a priori eliminated. Nevertheless, Brink's (1986) study does demonstrate that scattering by small-scale bumps can result in significant damping of the coherent wave field even in the presence of substantial density stratification. Thus, at present it is still unclear whether or not the free waves propagating past Nain Bank will maintain coherence further south along the shelf as they attempt to traverse the intervening abrupt large-scale topographic features.

The primary purpose of the work presented here is to examine this question from an observational viewpoint. Some insight is provided by the work of Middleton and Wright (1989). They used the mode fitting technique developed by Haines *et al.* (1990) to demonstrate the presence of free waves on the shelf. It is clear from their study that some wave energy does propagate from Nain Bank over substantial topographic irregularities to reach Hamilton Bank. However, their study does not extend to the Grand Bank (the data considered was restricted to the shelf region between Cape Chidley and Hamilton Bank). Their work also assumes that the wave energy is dominated by the Kelvin wave and the first two shelf wave modes, and that these modes propagate freely along the

shelf without being scattered by topographic variations. The limited success of this approach indicates that mode scattering and local forcing may be important. Such effects are investigated in the present paper through a statistical study using multiple regression techniques in the frequency domain.

The remainder of this report is as follows. The data sources are discussed in section 2 and a cursory description in terms of time series, spectra and complex empirical orthogonal functions is presented in section 3. In section 4 the statistical models and the dynamical ideas which motivate them are discussed. Detailed results are presented in section 5. A summary and discussion of results is given in section 6.

2. THE DATA SET

Between July, 1986 and August, 1987 the Bedford Institute of Oceanography collected an extensive set of data over the Labrador/Newfoundland Shelf (Fig. 1). The line across Hamilton Bank on Fig. 1 indicates the location of a CTD section occupied during the deployment and recovery of instruments. Figure 4 shows the density and buoyancy frequency along this section during August, 1986 and is typical of conditions at this time of year. The boxed crosses on Fig. 1 indicate the locations of bottom pressure measurements (the principal data set considered here) and the associated numbers will be used for reference in the text. Table 1 gives pertinent information for each of these pressure records.

The raw pressure records were dominated by diurnal and semi-diurnal tides. After checking (particularly for time errors), editing and despiking, the tidal constituents were obtained from harmonic analysis and removed (see Wright, *et al.*, 1988 for detailed tidal information). A Cartwright low pass filter, which passed essentially all of the energy at periods exceeding 2 days and less than 2% of the energy at periods less than one day, was applied and each record was decimated to a 6 hr sampling interval.

A geostrophic wind data set sampled six hourly and covering the period July, 1986 through August, 1987 was obtained from the Canadian Atmospheric Environment Service (AES) from which wind stress estimates were determined following Thompson *et al.* (1983) and Large and Pond (1981). We were later informed that a numerical model study of this region suggested that wind stress estimates obtained from the European Centre for Medium Range Weather Forecasts (ECMWF) were superior to the AES geostrophic estimates (Brad de Young, Memorial University, personal communication). All statistical results were re-calculated using the ECMWF wind estimates from the three stations indicated in Fig. 1, and these results are presented here. Qualitative conclusions were not affected by the choice of wind stress estimates but quantitative details did differ.

Six-hourly estimates of surface atmospheric pressure data were also obtained from AES for each of the Hudson Bay coastal towns of Coral Harbour, Moosonee, Inukjuak and Churchill. Following Wright, *et al.* (1987) the spatial

average of atmospheric pressure over Hudson Bay is estimated by the arithmetic mean of these four records.

3. A CURSORY DESCRIPTION OF THE DATA

Root-mean-square pressure variations over the array are presented in Fig. 5, revealing the general tendency for pressure variations to be of relatively uniform amplitude in the alongshelf direction and to decrease towards the shelf break. This is consistent with expectations based on both previous theoretical studies (eg. Clarke and Brink, 1985) and previous observations in other regions (eg., Brown *et al.*, 1985). However, Fig. 5 says nothing about the relationships between the various time series.

Figure 6, 7 and 8 show the bottom pressure time series across Nain, Hamilton and Grand Banks. There is visible coherence between records across each Bank, but the coherence clearly decreases with cross-shelf distance of separation, and it decreases rapidly across the shelf/slope boundary (see Fig. 7 in particular).

In Fig. 6 the spatial average of atmospheric pressure over Hudson Bay, and the alongshelf component of ECMWF wind stress from the central station in Fig. 1 are also shown. The relations between these forcing terms and the pressure variations at Nain were discussed in detail by Wright *et al.* (1987). Here, we simply note the obvious visual coherence between atmospheric pressure variations over Hudson Bay and the subsurface pressure variations over Nain Bank. Coherence with the local wind stress is less evident but not insignificant (see Wright *et al.*, 1987).

The pressure records from the four coastal stations in Fig. 1 are presented in Fig. 9. The gauges at Nain and St. John's are separated by a distance of roughly 1500 km. Finally, time series of bottom pressure for four gauges near the shelf break are presented in Fig. 10. Visual coherence over large alongshelf separation distances is evident in both figures.

For each time series shown in Figs. 6–10, corresponding auto spectra are presented in Figs. 11–15. The general decrease in energy levels with offshore distance is again evident. This is particularly true for periods between about 2 and 5 days (i.e., in the meteorological or Met Band), so that spectra become more red with offshore distance. The enhanced energy in the Met Band over the shelf is, in part, a natural consequence, of the blocking of the surface Ekman transport by the coastal wall together with the influence of the coastal wave guide (i.e., the generation of CTW's by local wind stress). On the Labrador Shelf, coastal trapping of motions generated by flow in and out through Hudson Strait also contributes to the enhancement of pressure variations over the shelf (Wright *et al.*, 1987).

Spectra across the Grand Bank contrast with those across the other Banks. The nearshore pressure signals in the Met Band are larger than those further up the shelf (Fig. 14), and the decrease from coastal to offshore values (Fig. 13) occurs more abruptly near the shelf break on the Grand Bank than on the other Banks.

Energy levels in the offshore are quite uniform along the shelf (Fig. 15) and show only a very weak indication

of increased energies in the Met Band. In this context it should be noted that the gauge represented by Fig. 15c, while at 360 m, is still inshore of the shelf break on the St. Anthony line. The suggestion of a somewhat larger signature of local meteorological forcing seen here compared to at the other offshore stations is thus to be expected.

Frequency-dependent empirical orthogonal functions (EOF's) have been calculated in order to better define the coherent pressure variations over the array. Figure 16 shows the percentage of variance over the 17 locations accounted for by the first two complex EOF's. These modes account for 80 to 90% of the variance over all frequencies below 0.5 cpd, and the first mode alone accounts for the majority of this variability. The amplitude and phase structures of this mode, for frequency bands centered on periods of 24, 8 and 4 days, are shown in Figs. 17–19.

In each band there is a general seaward decrease in amplitude. In the lowest frequency band near-shore amplitudes generally decrease in the alongshore direction of coastally trapped wave propagation, but in the other bands amplitudes increase in this direction. The phases suggest alongshore propagation in the direction expected for CTW's but the structures are certainly not consistent with any single dynamical mode. Phases vary substantially across the shelf and a unique alongshelf phase speed cannot be defined (reminiscent of the numerical results presented in Fig. 2).

The above results demonstrate conclusively that bottom pressure variations are strongly coherent over large horizontal distances. While this is a significant result, it does not provide any information about the underlying cause of the coherence. That is, we still do not know for sure whether the large scale coherence is due to wave propagation along the coastal wave guide or if it simply reflects large scale coherence in the dominant forcing mechanisms. For example, if the wind stress were strongly coherent over the scale of the array, the pressure variations at St. John's and Nain could be coherent even if all wave energy propagating southward past Nain was backscattered or dissipated before reaching St. John's.

To gain some feeling for the spatial structure of the wind field, complex EOF's were determined based on stress estimates at six stations along the shelf. These results demonstrated that the stress field is dominated by large scale disturbances (~50% of the variance over 12 time series is in mode 1 with an additional 20% in mode 2), but the spatial structure of these disturbances is nontrivial. In particular we note that the Grand Bank region is directly under a storm track which does not strongly influence the shelf further north.

4. STATISTICAL MODELS/SEPARATION OF REMOTELY AND LOCALLY FORCED MOTIONS

In this section we introduce regression models designed to separate pressure variations over the Labrador/Newfoundland Shelf into contributions which propagate into the region across the Nain section, contributions which enter across the shelf/slope boundary, and contributions which are generated locally by meteorological

forcing. In order to accomplish such a separation we require measures of the incoming coastally trapped wave field at Nain Bank, the offshore influence, and the local wind stress.

First, consider the CTW energy entering the domain across Nain Bank. This energy may be generated by wind stress over the shelf north of Nain, atmospheric pressure changes over Hudson Bay, deep ocean effects or any other mechanism. In this report we do not consider what forces these CTW's, but previous studies (Wright *et al.*, 1987; Webster and Narayanan, 1988; Middleton, 1988; Middleton and Wright, 1988, 1989) do suggest that the CTW response at Nain Bank is dominated by the first three dynamical modes (the deep ocean Kelvin Wave and 2 continental shelf wave modes). Originally, it was intended to use the data at Nain Bank to determine the dynamical modal amplitudes, using the method of Haines *et al.* (1990). Unfortunately, both dynamical modes 1 and 2 for Nain Bank have nodes in pressure between the outer two gauges (see Middleton and Wright, 1989), so the data from these sites did not significantly influence these modal amplitude estimates. Thus, the method of Haines *et al.* (1990) applied to the data across Nain Bank could lead to large errors in the estimated modal amplitudes. Because of this, alternative representations of the wave field at Nain Bank were considered.

At present, the source of pressure variations at the offshore sites on Nain Bank is unknown. They may, for example, be due to energy in the mode 3 continental shelf wave or they may be due to currents in the deep ocean. The latter possibility could result in pressure variations over the shelf which would be nearly independent of cross-shelf position. In the following discussion we will assume this to be the case. Evidence for the validity of this assumption will be given a posteriori.

With the assumption that the pressure variations seen at the outer two gauges are primarily due to a "deep ocean" mode, we estimated the amplitude of this mode by the average of the pressures at these two gauges (Fig. 20) and subtracted it from each of the four gauges across Nain Bank. The four residual time series (Fig. 21) are assumed to be associated with CTW modes.

In order to determine an optimal representation of the residual pressure variations across Nain Bank, complex EOF's were again calculated, this time on just the four residual time series. As indicated on Fig. 22, it was found that in all frequency bands, the first mode accounted for nearly all of the variance over the four sites (roughly 95%). The amplitudes and phases of this mode in three frequency bands are illustrated in Fig. 22. The amplitude looks very much like that of the first dynamical shelf wave mode. This is also true for the phase at the lowest frequency, but at higher frequencies, the rapid cross-shelf changes in phase (particularly between the middle two gauges) suggest that additional modes are also present. Note that the representation of two or more dynamical modes by one empirical mode is consistent provided the modes result from a common forcing mechanism. For example, coherent modes could be generated by the pumping of water in and out through Hudson Strait as a result

of pressure variations over Hudson Bay, or by the scattering of mode 1 wave energy as it passes over Hudson Canyon (Middleton and Wright, 1989). It should also be noted that the coherence between different dynamical modes at Nain Bank would make it very difficult, if not impossible, to use statistical analysis to separate energy found further south into contributions arising from the different modes at Nain Bank.

In the following, the empirical mode illustrated in Fig. 22 is referred to as mode 1 (m_1) and the mode represented by the average of the pressures observed at the outer two gauges is referred to as mode 2 (m_2).

Finally, we need some measure of local wind stress forcing. As discussed in section 3, the wind stress over the Labrador/Newfoundland Shelf is dominated by large scale disturbances, but there is substantial variation between Nain and St. John's. Three ECMWF wind stress time series were chosen to represent the northern central and southern parts of this area (Fig. 1). These wind stress estimates are referred to as τ_1, τ_2 and τ_3, respectively.

Assuming that the observed pressure variations are due to a combination of CTW energy entering across Nain Bank (m_1), forcing by motions in the deep ocean (m_2), and local forcing by wind stress (τ_1,τ_2, τ_3), and assuming that the dynamics are essentially linear, we consider the multiple regression model

$$P_i = a_{i1}M_1 + a_{i2}M_2 + a_{i3}T_1^x + a_{i4}T_1^y + a_{i5}T_2^x + a_{i6}T_2^y + a_{i7}T_3^x + a_{i8}T_3^y + \epsilon_i,$$

or simplifications obtained by setting some of the coefficients, a_{ij}, equal to zero. In (1), P_i, M_1, M_2, T_k^x, T_k^y are the Fourier transforms of the corresponding time series $p_i, m_1, m_2, \tau_k^x, \tau_k^y$. Minimizing $|\epsilon_i|^2$ with respect to the complex coefficients a_{ij}, j=1, 2, . . . , 8 gives a set of linear equations for each frequency band which determines these coefficients (see Wunsch (1972) for further discussion). The magnitudes and phases of the coefficients give the estimated gains and phases of the bottom pressure response at station i with respect to each of the assumed forcing terms.

5. REGRESSION RESULTS

In this section we consider the statistical predictions based on the various forms of the regression model, (1).

In Tables 2a, b, c we show the residual variance in our three primary frequency bands based on regression models of the form (1) but with only the inputs given at the top of each column. The first four columns are included to show how much variance can be accounted for by using simplified statistical models. The second last column corresponds to the full model (1), while the last column gives the results from a simplified model in which the three separate wind stress estimates were replaced by their mean value. While there was some loss of information when this simplification was made, qualitative results did not change.

The results for M_1 alone are qualitatively as expected. Eighty percent of the variance is accounted for at the coastal gauge on Nain Bank but this percentage falls off very substantially in both the alongshelf and cross-shelf directions. It reduces to 10% or less at sites beyond the shelf break (notably at the deepest gauge on Nain Bank), which supports our expectation that the deep water pressure variations are not dominated by continental shelf waves.

Next, consider the results for M_2 (the 'offshore influence') alone. Most of the energy at the two seaward gauges on Nain Bank is accounted for by this input. Recalling that M_2 is simply formed by taking the average over these two gauges, the high percentage of variance explained here is simply a reflection of the high degree of coherence between these sites. The variance accounted for by M_2 at the other sites is perhaps more interesting. In particular we note that M_2 actually appears to be more useful than M_1 as a predictor of pressure variations over the array. This conflicts with the idea that continental shelf waves dominate the pressure variations over the shelf. M_1 and M_2together can account for a substantial fraction of the variance at nearly all sites, in each frequency band.

The variance accounted for by the three wind stress inputs (6 components) generally increases southward along the shelf and tends to be greatest near the coast. This is qualitatively as expected if the wind stress generates continental shelf waves which propagate southward along the shelf. Across the Grand Bank the wind stress alone accounts for somewhat more variance than M_1 and M_2 together.

Finally, as expected, the full model including M_1, M_2 and the three wind stresses, explains the most variance. This model accounts for 80% or more of the variance at coastal and near-shore sites, and a large part of the variance at all sites.

The results presented in Table 2 which are based on simplifications of (1) reflect statistical relations between the various variables but no direct cause and effect relations are implied. On the other hand, the full model accounts for all of the anticipated major forcing terms, and the cross-correlations between them. We can at least speculate on cause and effect based on model (1). Note, however, that this model does not account for all of the variance in the pressures. If there are important forcing terms which have not been accounted for and which are coherent with our chosen inputs, the gains estimated from (1) could be in error. Further, errors in the inputs themselves will result in uncertainties in the model results. With regard to this point we note that: (1) the influence of local wind stress is allowed for through rather crude estimates based on winds at just three points; (2) any "offshore influence" is accounted for solely through M_2, and; (3) the influence of continental shelf waves propagating into the region is represented solely by M_1. Any CTW energy crossing the Nain Bank section which is not coherent with M_1 is either ignored or included in M_2. The latter possibility is particularly important. Although we have referred to M_2 as the "offshore influence", it could simply represent coastal trapped wave energy not included in M_1. However, the results presented below indicate that this is not the case and that M_2 does represent an offshore influence.

Tables 3a, b, c show results for the full model given by (1). Each column shows that percentage of total energy that would remain if all but the indicated forcing term were shut off. For example the percentage of energy in p_i associated with M_1 is given by $100\times \mid a_{1i} \mid^2 \times$ Energy in m_1/Energy in p_i. These estimates are presented for each of our primary frequency bands. Note that since there can be interference (constructive or destructive) between the individual responses, the sum of the energies associated with the six inputs need not add up to the total energy accounted for: it could be larger or smaller. The sum of the energy percentages associated with individual forcing terms and the percent residual variance are given in the last two columns.

It is immediately clear from Table 3 that M_1 and M_2 represent important forcing mechanisms in all three frequency bands. The response associated with M_2 remains of similar importance over the full north-south extent of the array. The response associated with M_1 clearly diminishes to the south, particularly at higher frequencies.

T_1^τ, T_2^τ and T_3^τ account for less than 15% of the variance in each frequency bands for sites 1–12. T^τ appears to be more important to the low frequency variations near the shelf break on the Grand Bank (sites 16, 17). T_1^τ, T_2^τ and T_3^τ represent important forcing mechanisms in all three frequency bands. The lack of any significant response to wind stress at Nain Bank is particularly interesting. It suggests that if wave energy generated by the local wind stress is backscattered, it does not result in significant pressure variations at Nain Bank. Either there is little backscattering or backscattered energy is dissipated before reaching Nain Bank.

Figures 23–34 illustrate the spatial structure of the amplitudes and phases of the response associated with the four assumed forcing mechanisms in the three primary frequency bands. They are essentially maps of the magnitudes and phases of the regression coefficients. For example, to generate Fig. 23, a_{1j}, $j = 1, ..., 17$ for the frequency band centered on the 24 day period were used.

Figures 23–25 illustrate the spatial structure associated with M_1 for the three frequency bands considered. These results are qualitatively consistent with expectations based on theoretical (analytical and numerical) models. In general the amplitudes decay away from the coast and, at least near shore, phase changes indicate propagation from north to south. The amplitude decays much more rapidly than would be expected from frictional dissipation alone, suggesting that mode scattering into small-scale waves, which are more effectively dissipated, may be important. Wave scattering into smaller scale motions will also result in rapid phase changes with frequency. This effectively amounts to scattering into incoherent motions when averaging over a frequency band of finite width. Finally, the cross-shelf phase changes are much larger than would be expected from frictional dissipation alone (Brink and Allen, 1978). These results are at least qualitatively consistent with the numerical results presented in Fig. 3 for wave propagation over a realistic, rugged Labrador/Newfoundland Shelf.

Figures 26–28 illustrate the spatial structures associated with M_2 in the three frequency bands. The amplitude

of this mode is nearly uniform and the phase varies by 20° or less over the whole shelf. Indeed, at the 90% confidence level, we cannot say that either the amplitude or the phase varies significantly over the domain. This is certainly unlike the structure expected for CTWs. There is, however, some suggestion that amplitude increases slightly toward the coast and that phase increases slightly to the south in the higher two frequency bands, particularly for periods near four days. The results can be compared with expectations based on idealized models for the response of a shelf to pressure variations applied at the offshore boundary (Wright, 1986; Chapman and Brink, 1987; Power *et al.*, 1988). These studies show that for a steady pressure gradient applied at a deep ocean boundary the pressure response decreases towards the shore, but at non-zero frequencies the forcing may excite CTWs on the shelf. If the forcing matches the structure of a free CTW sufficiently closely, the response over the shelf can be dominated by the near-resonant excitation of this wave. It seems possible that the slight increase in amplitude toward the coast in the four day band is due to the relatively weak excitation of CTWs by a pressure gradient imposed in the "deep ocean".

It should be noted here that our "deep ocean" influence is represented by the pressure variations observed near the 400 m isobath. The lack of any decay toward the coast in our lowest frequency band may be due in part to the fact that M_2 does not strictly correspond to a deep ocean site. Further, the small phase changes over a distance of order 1500 km indicates that the forcing scales are very large. Wright (1986) suggests that even for steady forcing, a depth change δh will be penetrated by a deep ocean pressure gradient if

$$|\ell| < r/f\,\delta h\,w$$

where $|\ell|$ is the magnitude of the alongshore wavenumber of the forcing, r is a bottom friction coefficient, f is the local Coriolis parameter, and δh is the change in depth over the width w. For $r \sim 5 \times 10^{-4} m\,s^{-1}$, $f \sim 10^{-4} s^{-1}$, $\delta h \sim 400\,m$ and $w \sim 20\,km$ this requires

$$|\ell| < 6.2 \times 10^{-7}\,m^{-1}.$$

That is, the alongshore scale $(|\ell|^{-1})$ must exceed 1600km. Figures 26–28 suggest a longshore scale of order (360/20) ·1500 km/$2\pi \sim 4300km$. The 400 m change in depth is thus expected to be easily penetrated at these very low frequencies. The results for M_2 clearly suggest that pressure variations over the shelf are influenced by pressure variations beyond the shelf break. The origin of the latter is uncertain. The tendency for the amplitude of M_2 to decay seaward of the shelf break suggests that the origin might actually be over the slope and not the deep ocean. However, the reduced amplitude in deeper water could be a result of baroclinic compensation at depth or simple continuity requiring larger currents in shallow water than in deep water. Current and bottom pressure

data recently collected by the Bedford Institute on a line extending from Hamilton Bank out to the center of the Labrador Sea should help shed light on this question. One might also speculate that the "deep ocean" influence is related to the variation in current resulting from large scale wind stress changes over the North Atlantic (Thompson *et al.*, 1986; Greatbatch *et al.*, 1990). Comparison with results of numerical models such as that considered by Greatbatch *et al.* (1990) would be useful.

Figures 29–31 show the spatial structure of bottom pressure variation associated with the cross-shelf wind stress component. All estimates with a phase uncertainty of 180° are not significantly different from zero at the 90% confidence level. Note that the small gains at the Nain Bank section suggest the possibility that part of the response to τ^x has been incorporated into the response to the empirical mode m_1. Further, the phases of the response to τ^x are peculiar, suggesting a set-up generally lagging behind an offshore stress. It seems likely that even where error bounds suggest otherwise, the estimated response to τ^x is not reliable. However, it is also possible that the peculiarity of these gains is an indication that we have not accounted for some important forcing mechanism which is coherent with τ^x.

Figures 32–34 illustrate the spatial structure associated with τ^y. In the lowest frequency band (24 days) the gains are small and generally not statistically significant. On the other hand, there is some suggestion that amplitudes increase towards the coast and to the south, and higher pressures are associated with southward wind stress. These same characteristics are also seen in Figs. 33 and 34 where results are statistically significant.

6. DISCUSSION AND CONCLUSIONS

In an earlier report, Middleton and Wright (1989) presented results of a dynamical mode fitting exercise based on 10 pressure records over the upper part of the Labrador Shelf (between Saglek Bank and Hamilton Bank). In that report, pressure variations due to local wind forcing and deep ocean effects were assumed small and neglected. Further, all energy originally in one dynamical mode was assumed to remain in that mode even as the waves traversed the rugged topography of the Labrador Shelf. This assumption contrasts with speculation that pressure variations at Saglek Bank might be incoherent with pressure variations at Hamilton Bank due to scattering of energy into smaller scale waves which could carry the energy backward along the shelf. Results presented by Middleton and Wright (1989) clearly show that this process does not dominate the dynamics of pressure variations over the Labrador Shelf, and that simple wave propagation can carry information large distance along even this rugged shelf. On the other hand, their results also showed that some processes not included in the fitting procedure are important to the dynamics of this region. Obvious candidates include local wave generation by wind stress, offshore influences and mode scattering.

In this report we have taken an approach which is different from that considered by Middleton and Wright (1989). We have used complex empirical orthogonal functions to illustrate the dominant spatial structure of pressure variations in this region, and frequency-dependent regression models to help clarify the importance of the processes neglected in the earlier study.

The main result of the EOF analysis is that pressure variations over the Labrador Shelf are strongly correlated over cross-shelf distances of order 100 km and alongshelf distances of order 1000 km. The spatial structure of the first empirical mode suggests that the first dynamical mode dominates the pressure field but additional modes are also important.

Our analysis demonstrated clearly that coastally trapped waves entering the area from the north, the "offshore" influence, and local forcing by wind stress are all important over at least some part of the region considered. The combination of these influences accounts for much of the sub-tidal variance at all sites and 80% or more of the variance at the near-shore sites. While this performance is encouraging, it is natural to ask what effects have been neglected which result in motions incoherent with the assumed forcing mechanisms. One obvious candidate, particularly for the sites in the vicinity of the offshore branch of the Labrador Current, is instabilities of this current. LeBlond (1982) shows evidence of such instabilities from satellite photos, and based on idealized models suggests that they result from baroclinic instability. The associated motions would likely have pressure signals similar to the spatial structure of our residuals so we believe this is a prime candidate. Further, LeBlond's (1982) observations, as well as expectations based on idealized models, suggest that currents associated with such instabilities may be significant. Clearly further study of this process is warranted.

Other limitations of our regression model may well be dominated by inadequacies in our representation of the assumed forcing mechanisms. The representations of wind stress forcing and offshore influences are particularly open to criticism. Wind stress is represented by at most three averaged values representing the northern, central and southern parts of the shelf. While examination of the stress field using empirical orthogonal functions shows that much of the wind energy is in large scale features, our representation is clearly an over-simplification. To provide a significantly improved representation will probably require the use of observed winds in numerical studies of the region. Such studies are presently in progress (deYoung and Greatbatch, Memorial University, St. John's, Nfld.; pers. comm.). Our representation of the "offshore influence" is also crude: we simply represent it by the pressure variations observed at a location where coastal trapped wave energy is expected to be minimal. We hope that ongoing numerical studies will help clarify this aspect also.

Qualitative results for each forcing function are summarized below.

The spatial structures associated with M_1 (the dominant empirical mode at Nain Bank) clearly support the

conclusion of Middleton and Wright (1989) that coastally trapped waves play an important role in determining the pressure field over the Labrador/Newfoundland Shelf. On the other hand, the large decrease in amplitude with distance down the shelf suggests that energy is scattered into smaller scale motions which are either more effectively dissipated by bottom friction or degrade the coherence when results are band averaged to obtain statistical reliability. In either case, it is clear that wave scattering is an important process, as anticipated by previous theoretical (see the references discussed in §1) and numerical studies (Fig. 2).

In considering the details of Figs. 23–25 some cautionary comments are warranted. The main cause of concern is that these structures correspond to an empirical mode at Nain Bank, not a dynamical mode. While the cross-shelf structure at Nain Bank supports the conclusion of Wright *et al.* (1987) and Webster and Narayanan (1988) that the first dynamical mode dominates the pressure field there, other coherent motions will also be incorporated into this empirical mode. Thus, the cross-shelf phase changes in Figs. 23–25 could reflect phase interference between different dynamical modes rather than mode scattering. Mode scattering must, however, be important to explain the large decrease in down-shelf energy flux between the section across Nain Bank and the section across the Grand Bank (compare Fig. 2a where mode scattering is small to Fig. 2b where it is strong and note that the latter more clearly resembles the results presented in Figs. 23–25).

The results for M_2 (the "offshore" influence) are potentially important, not so much for understanding shelf dynamics as for figuring out what can be said about the deep ocean based on coastal sea level measurements (Thompson *et al.*, 1986; Greatbatch *et al.*, 1990). Figures 26–28 suggest that the pressure variations observed near the shelf break are due to an "offshore" influence rather than CTW's, and Table 3 shows that this influence is important over the whole domain, particularly in the lowest and highest frequency bands we considered.

The response to cross-shelf wind stress is expected to be relatively small ($\sim 0.1 mPa^{-1}$: see Wright *et al.*, 1987). This is generally consistent with results presented in Figures 29–31. In the lowest frequency band, there is no statistically significant response at the 90% confidence level, but it should be noted that the degrees of freedom for this band is just one-third of that in the higher bands. While the response is weak, as expected, the phase of the response is not consistent with expectations (we expected sea level to be roughly 180° out of phase with cross-shelf stress as found by Wright *et al.*, 1987). This peculiar response may be due in part to our crude representation of wind stress variations. Since the cross-shelf and alongshelf stress components are statistically related, our crude representation of the stress field may have resulted in some of the pressure variations due to alongshelf stress being incorrectly related to the cross-shelf component. Other possibilities are that the peculiar response could be a result of the irregular shelf topography or due to the influence of Hudson Strait and Belle Isle Strait.

Finally, the response to alongshelf stress (Figs. 32–34) shows the expected increase southward from Nain

Bank, at least at the higher frequencies (results from the lowest band are again not reliable at the 90% confidence level). Also, phase indicates higher pressures lagging southward directed stress as expected.

While the results presented here clearly reveal that wind stress is an important factor in determining pressure variations along the Labrador Shelf, the picture is by no means simple. The evidence from both numerical and statistical models indicates that there is strong scattering of the wave field as a result of abrupt topographic variations. A detailed analysis of model and data from a region of strong topographic variations is clearly called for.

REFERENCES

Anderson, C., 1986. Motions driven by buoyancy forces and atmospheric stresses in the Avalon Channel, Newfoundland, Canada, Ph.D. Thesis, McGill University, 196 pp.

Anderson, D.L.T. and R.A. Corry, 1985. Seasonal transport variations in the Florida Straits: A Model Study. *J. Phys. Oceanogr.*, **15**, 773–786.

Brink, K.H., 1986. Scattering of long coastal-trapped waves due to bottom irregularities. *Dyn. Atmos. Oceans*, **10**, 149–164.

Brink, K.H. and J.S. Allen, 1978. On the effect of bottom friction on barotropic motion over the continental shelf. *J. Phys. Oceanogr.*, **8**, 919–922.

Brown, W.S., Pettigrew, N.R., and J.D. Irish, 1985. The Nantucket Shoals flux experiment (NSFE79). Part II: The structure and variability of across-shelf pressure gradients. *J. Phys. Oceanogr.*, **15**, 749–771.

Chapman, D.C., 1983. On the influence of stratification and continental shelf and slope topography on the dispersion of subinertial coastally trapped waves. *J. Phys. Oceanogr.*, **13**, 1641–1652.

Chapman, D.C. and K.H. Brink, 1987. Shelf and slope circulation induced by fluctuating offshore forcing. *J. Phys. Oceanogr.*, **92**, 11,741–11,759.

Clarke, A.J. and K.H. Brink, 1985. The response of stratified frictional flow of slope and shelf waters to fluctuating large-scale, low-frequency wind forcing. *J. Phys. Oceanogr.*, **15**, 439–453.

deMargerie, S., 1985. Barotropic tidal circulation of the Scotian Shelf. Contract Rep. OSC 84–00218, Can. Hydrogr. Serv., Dartmouth, N.S.

Garrett, C.J.R., Majaess, F. and B. Toulany, 1985. Sea-level response at Nain, Labrador, to atmospheric pressure and wind. *Atmos.-Ocean*, **23**(2), 95–117.

Greatbatch, R.J., deYoung, B., Goulding, A. and J. Craig, 1990. On the influence of local and North Atlantic wind forcing on the seasonal variation of sea level on the Newfoundland and Labrador Shelf. *J. Geophys. Res.*, **15**, 5279–5289.

Greenberg, D.A., 1983. Modelling the mean barotropic circulation in the Bay of Fundy and Gulf of Maine. *J. Phys. Oceanogr.*, **13**, 886–904.

Haines, J., Thompson, K.R. and D. Weins, 1991. The detection of coastal trapped waves. J. Geophys. Res., In press.

Huthnance, J.M., 1978. On coastal trapped waves: Analysis and numerical calculations by inverse iteration. *J. Phys. Oceanogr.*, **8**, 74–92.

Large, W.G. and S. Pond, 1981. Open ocean momentum flux measurements in moderate to strong winds. *J. Phys. Oceanogr.*, **11**, 324–336.

LeBlond, P.H., 1982. Satellite observations of Labrador Current undulations. *Atmos.-Ocean*, **20**(2), 129–142.

Middleton, J.F., 1988. Longshelf waves generated by a coastal flux. *J. Geophys. Res.*, 93(C9), 10,724–10,730.

Middleton, J.F. and D.G. Wright, 1988. Shelf wave scattering due to a longshore jump in topography. *J. Phys. Oceanogr.*, **18**, 230–242.

Middleton, J.F. and D.G. Wright, 1989. Coastally trapped waves on the Labrador Shelf. *Can. Tech. Rep. Hydrogr. Ocean Sci.*, No. 116: vi + 76 pp.

Power, S.B., Middleton, J.H., and R. Grimshaw, 1988. Frictionally modified continental shelf waves and the sub-inertial response to wind and deep ocean forcing. Applied Mathematics Preprint, University of New South Wales, 41 pp.

Schwiderski, E., 1980. On charting global ocean tides. *Rev. Geophys.*, **18**, 243–268.

Thompson, K.R., Marsden, R.F. and D.G. Wright, 1983. Estimation of low-frequency wind stress fluctuations over the open ocean. *J. Phys. Oceanogr.* **13**, 1003–1011.

Thompson, K.R., Lazier, J.R.N. and B. Taylor, 1986. Wind-forced changes in Labrador Current transport. *J. Geophys. Res.*, 91(C12), 14,261–14,268.

Wang, D.-P., 1980. Diffraction of continental shelf waves by irregular alongshore geometry. *J. Phys. Oceanogr.*, **10**, 1187–1199.

Webster, I., 1987. Scattering of coastally-trapped waves by changes in shelf width. *J. Phys. Oceanogr.*, **17**, 928–937.

Webster, I. and S. Narayanan, 1988. Low-frequency current variability on the Labrador Shelf. *J. Geophys. Res.*, 93(C7), 8163–8173.

Wilkin, J. and D.C. Chapman, 1987. Scattering of continental shelf waves at a discontinuity in shelf width. *J. Phys. Oceanogr.*, **17**, 713–724.

Wilkin, J. and D.C. Chapman, 1988. Scattering of coastal-trapped waves by irregularities in coastline and topography. EOS-Transactions of the American Geophysical Union, 69(44), 1277.

Wright, D.G., 1986. On quasi-steady circulation driven by alongshelf wind stress and open-ocean pressure gradients. *J. Phys. Oceanogr.*, **16**, 1712–1714.

Wright, D.G., Greenberg, D.A. and F.G. Majaess, 1987. The influence of bays on adjusted sea level over adjacent shelves with application to the Labrador Shelf. *J. Geophys. Res.*, **92**(C13), 14,610–14,620.

Wright, D.G., Lazier, J.R.N. and W. Armstrong, 1988: Moored current and pressure data from the Labrador/Newfoundland Shelf, June 1985 – July 1987. *Can. Data Rep. Hydrogr. Ocean Sci.*, No. 62: x + 258 pp.

Wunsch, C., 1972. Bermuda sea level in relation to tides, weather and baroclinic fluctuations. *Rev. Geophys.*, **10**, 1–49.

APPENDIX: The Numerical Model

The equations of continuity and motion used in the numerical model are:

$$\frac{\partial \zeta}{\partial t} - \frac{1}{R\cos\theta}\left[\frac{\partial}{\partial \Phi}(h+\zeta)u - \frac{\partial}{\partial \theta}\cos\theta\,(h+\zeta)v\right] = 0 \tag{1}$$

$$\frac{\partial u}{\partial t} - \frac{u}{R\cos\theta}\frac{\partial u}{\partial \Phi} + \frac{v}{R}\frac{\partial u}{\partial \theta} - \frac{uv\tan\theta}{R}$$

$$= v\,2\omega\sin\theta + \frac{g}{R\cos\theta}\frac{\partial \zeta}{\partial \Phi} - Ku\frac{(u^2+v^2)^{\frac{1}{2}}+V}{h+\zeta} +$$

$$+ \frac{Ah}{R^2\cos^2\theta}\frac{\partial^2 u}{\partial \Phi^2} + \frac{Ah}{R^2}\frac{\partial^2 u}{\partial \theta^2} - \frac{Ah\tan\theta}{R^2}\frac{\partial u}{\partial \theta} \tag{2}$$

$$\frac{\partial v}{\partial t} - \frac{u}{R\cos\theta}\frac{\partial v}{\partial \Phi} + \frac{v}{R}\frac{\partial v}{\partial \theta} + \frac{u^2\tan\theta}{R}$$

$$= -u\,2\omega\sin\theta - \frac{g}{R}\frac{\partial \zeta}{\partial \theta} - Kv\frac{(u^2+v^2)^{\frac{1}{2}}+V}{h+\zeta} +$$

$$+ \frac{Ah}{R^2\cos^2\theta}\frac{\partial^2 v}{\partial \Phi^2} + \frac{Ah}{R^2}\frac{\partial^2 v}{\partial \theta^2} - \frac{Ah\tan\theta}{R^2}\frac{\partial v}{\partial \theta} \tag{3}$$

Where:

ζ — sea surface elevation

t — time

R — the earth' s radius

θ — latitude

Φ — longitude

u — eastward velocity

h — still water depth

ω — angular rate of the earth's rotation

g — gravitational acceleration

K — bottom friction coefficient

Ah — horizontal eddy viscosity coefficient

v — northward velocity

V — background current speed

The finite difference scheme used is similar to that employed in the fine grid model described in Greenberg (1983) but adapted to spherical polar coordinates by deMargerie (1985). Damping is accounted for by the inclusion of three different parameters: the bottom friction coefficient (K=0.0025), the mean background current speed (V=0.2 $m \cdot s^{-1}$) which crudely represents the damping effects of unmodelled currents (e.g. tidal constituents and unmodelled wind effects), and the horizontal eddy viscosity coefficient (Ah=0.4•h $m^2 s^{-1}$). This depth dependent form of Ah is similar to that used by Schwiderski (1980) and is effective in damping out spurious motion in deep water where bottom friction has little effect. Motions on a horizontal scale of 10 (100) km are damped by this term over a time scale of order 14(1400) days in water 200 m deep and ~10 times faster in water 2000 m deep.

Along coastal boundaries the normal velocity is set to zero. On the northern open boundary, a sinusoidal tide-like elevation was prescribed with amplitude varying linearly from 10 cm at the coast to zero at the shelf break and phase uniform, with the period of oscillation prescribed to match the frequency band being examined. From the shelf break to the eastern open boundary, runs were made with either elevation set to zero or using the radiation condition:

$$U_h = Z_b \sqrt{(g/h)}$$

where U_h is the velocity component normal to the open boundary and Z_b is the calculated elevation next to the boundary. The Strait of Belle Isle was considered to be a closed (land) boundary, but was tested with a radiation condition which showed similar results except very near the Strait. The remaining open boundaries all used the radiation condition.

Different cross–shelf forms of the northern boundary condition produced results that were quantitatively quite different but qualitatively similar. This is consistent with the results of the fitting of the data to empirical modes which indicated a strong offshore influence (see Section 5 — Regression Results). Given the limitations of the model and the data, it was not thought to be productive to tune the model in an attempt to define a "correct" off-shelf influence.

The model depths were digitized on a grid one-third of a degree in latitude by one-fifth of a degree in longitude interpolated from available depths to a regular grid (using data and programs graciously provided by ASA Consulting, Dartmouth, N.S.). These depths were then smoothed as described in the text.

Table 1. Pressure gauge information.

Site Number	Latitude	Longitude	Water Depth (m)	Start Date	Length (Days)
1	56.53°N	61.68°W	4	5/8/86	381
2	56.54°N	60.33°W	201	8/8/86	357
3	56.94°N	59.30°W	157	8/8/86	357
4	57.03°N	58.95°W	570	9/8/86	358
5	54.46°N	55.44°W	200	5/8/86	360
6	53.63°N	55.83°W	80	4/8/86	360
7	53.73°N	55.45°W	200	4/8/86	360
8	53.84°N	55.18°W	153	4/8/86	360
9	53.73°N	53.62°W	200	3/8/86	354
10	54.03°N	52.78°W	1007	3/8/86	355
11	54.17°N	52.13°W	2480	2/8/86	356
12	51.37°N	55.58°W	17	3/8/86	381
13	51.67°N	52.99°W	360	27/7/86	360
14	47.47°N	52.77°W	8	30/8/86	378
15	47.40°N	51.80°W	183	20/4/86	387
16	46.83°N	48.72°W	98	21/4/86	381
17	46.42°N	47.27°W	402	14/10/86	206

Table 2a. Residual variance for various statistical models. Period = 24 days.						
Forcing / Site Number	M1	M2	M1, M2	$\tau_{1,2,3}$	M1, M2, $\tau_{1,2,3}$	M1, M2, τ
1	20	51	0.2	64	0.1	0.2
2	45	26	1	71	1	1
3	80	5	3	75	1	2
4	98	6	3	53	2	3
5	52	33	11	72	7	8
6	41	47	14	62	4	6
7	58	26	9	71	3	5
8	58	34	15	75	8	12
9	88	42	40	79	27	36
10	89	23	20	54	10	18
11	91	54	42	52	20	31
12	67	45	30	65	19	22
13	97(94)	29(21)	28(21)	35(31)	14(10)	26(18)
14	77	58	47	21	10	18
15	69	55	33	24	8	16
16	60	66	27	38	16	22
17	89	58	51	34	32	37

Two values are given for Site 13 (located offshore of St. Anthony) in Tables 2 and 3. The first value is based on 309 days of data as are all values for Sites 1-12, while the second value is based on 195 days of data as are all values for Sites 14-17.

Table 2b. Residual variance for various statistical models. Period = 8 days.						
Forcing / Site Number	M1	M2	M1, M2	$\tau_{1,2,3}$	M1, M2, $\tau_{1,2,3}$	M1, M2, τ
1	21	59	1	60	1	1
2	44	50	5	65	3	3
3	76	12	6	68	4	5
4	98	20	9	81	6	8
5	56	63	32	49	17	22
6	48	69	31	33	8	11
7	75	52	39	56	20	25
8	75	53	42	61	26	72
9	89	77	71	84	62	68
10	99	55	47	80	34	41
11	94	68	53	82	45	49
12	66	77	53	35	21	24
13	98(98)	63(62)	60(61)	69(54)	36(28)	55(56)
14	80	73	62	12	6	20
15	77	77	62	21	13	32
16	70	87	64	54	38	46
17	100	83	81	76	43	63

Table 2c. Residual variance for various statistical models. Period = 4 days.						
Forcing / Site Number	M1	M2	M1, M2	$\tau_{1,2,3}$	M1, M2, $\tau_{1,2,3}$	M1, M2, τ
1	6	58	.4	34	.2	.3
2	20	41	3	43	2	2
3	72	9	6	44	4	6
4	83	14	10	61	7	9
5	48	43	24	33	15	18
6	53	40	26	19	7	9
7	48	37	20	26	11	13
8	55	33	20	37	15	18
9	87	51	50	61	38	40
10	84	38	31	72	26	27
11	88	45	37	66	35	37
12	67	48	40	22	10	15
13	83(80)	74(80)	68(71)	40(41)	21(22)	49(56)
14	69	55	46	10	5	14
15	73	57	48	13	8	15
16	89	81	77	26	25	35
17	90	77	73	62	25	41

Table 3a. % variance that would occur if each forcing term was taken to act in isolation. Results determined by the model: $P_i = a_1 M_1 + a_2 M_2 + a_3 t_1^x + a_4 t_1^y + a_5 t_2^x + a_6 t^x + a_7 t_3^x + a_8 t_3^y + \epsilon$. Period = 24 days

Forcing Site Number	M_1	M_2	τ_1^x	τ_1^y	τ_2^x	τ_2^y	τ_3^x	τ_3^y	Σ	Residual
1	59	21	0	0	0	0	0	0	80	0.1
2	25	50	0	1	0	0	0	0	76	1
3	1	101	0	2	0	1	1	1	107	1
4	1	88	1	2	0	1	1	1	95	2
5	14	58	0	6	0	0	0	0	78	7
6	21	42	0	5	1	2	0	1	72	4
7	21	52	1	5	2	0	1	0	82	3
8	28	44	1	7	2	0	2	0	84	8
9	3	71	1	13	8	8	0	3	107	27
10	3	74	0	10	3	14	14	2	120	10
11	11	36	4	31	13	6	1	4	106	21
12	8	49	2	3	0	2	3	0	67	19
13	6(7)	52(36)	1(4)	4(7)	3(7)	18(2)	2(15)	10(0)	96(73)	14(8)
14	4	26	5	3	3	4	5	11	61	5
15	12	26	2	3	5	9	6	8	71	7
16	60	12	2	10	30	15	15	3	147	15
17	8	12	5	34	33	0	15	3	110	26

Table 3b. % variance remaining if each forcing term was taken to act in isolation. Results determined by the model: $P_i = a_1 M_1 + a_2 M_2 + a_3 \tau_1^x + a_4 \tau_1^y + a_5 \tau_2^x + a_6 \tau^x + a_7 \tau_3^x + a_8 \tau_3^y + \epsilon$. Period = 8 days

Forcing / Site Number	M_1	M_2	τ_1^x	τ_1^y	τ_2^x	τ_2^y	τ_3^x	τ_3^y	Σ	Residual
1	76	20	0	0	0	0	0	0	96	0.6
2	47	46	2	0	0	0	0	0	95	3
3	4	76	0	2	0	1	0	1	84	4
4	6	95	0	4	0	1	0	1	107	6
5	14	29	2	11	1	0	0	1	58	17
6	15	20	2	11	1	2	0	0	51	8
7	4	43	4	8	1	0	1	0	61	20
8	4	40	4	6	2	1	1	0	58	26
9	6	22	2	0	1	77	4	5	117	62
10	4	58	3	13	5	5	1	1	90	34
11	13	43	0	1	6	2	2	3	70	45
12	6	12	1	7	1	8	3	2	40	21
13	6(9)	41(29)	3(3)	5(13)	1(2)	7(4)	9(19)	1(1)	72(80)	36(28)
14	1	7	0	6	0	8	11	15	48	6
15	2	9	6	1	1	9	3	15	46	13
16	10	13	15	0	1	24	2	1	66	38
17	10	38	17	21	1	11	0	6	104	43

Table 3c. % variance remaining if each forcing term was taken to act in isolation. Results determined by the model: $P_i = a_1 M_1 + a_2 M_2 + a_3 \tau_1^x + a_4 \tau_1^y + a_5 \tau_2^x + a_6 \tau_2^y + a_7 \tau_3^x + a_8 \tau_3^y + \epsilon$. Period = 4 days

Forcing Site Number	M_1	M_2	τ_1^x	τ_1^y	τ_2^x	τ_2^y	τ_3^x	τ_3^y	Σ	Residual
1	75	7	0	0	0	0	0	0	82	0.2
2	44	20	1	0	0	0	0	0	67	2
3	2	77	1	0	0	1	1	2	84	4
4	4	104	1	0	0	1	1	3	114	7
5	14	21	4	4	0	1	0	0	44	15
6	6	17	3	10	1	3	0	1	41	7
7	9	20	2	5	0	2	0	0	38	11
8	10	33	1	3	0	2	0	0	49	15
9	1	43	1	1	4	12	1	1	74	38
10	4	89	0	6	0	0	0	4	103	26
11	7	59	0	1	1	2	1	1	72	35
12	3	18	3	1	2	12	4	3	46	10
13	2(3)	35(41)	6(9)	6(7)	3(2)	4(4)	14(25)	6(4)	76(95)	21(22)
14	1	11	2	4	0	3	5	22	48	5
15	0	12	2	5	4	14	6	7	50	8
16	1	2	1	7	8	37	10	19	85	25
17	3	86	2	2	6	0	11	37	147	25

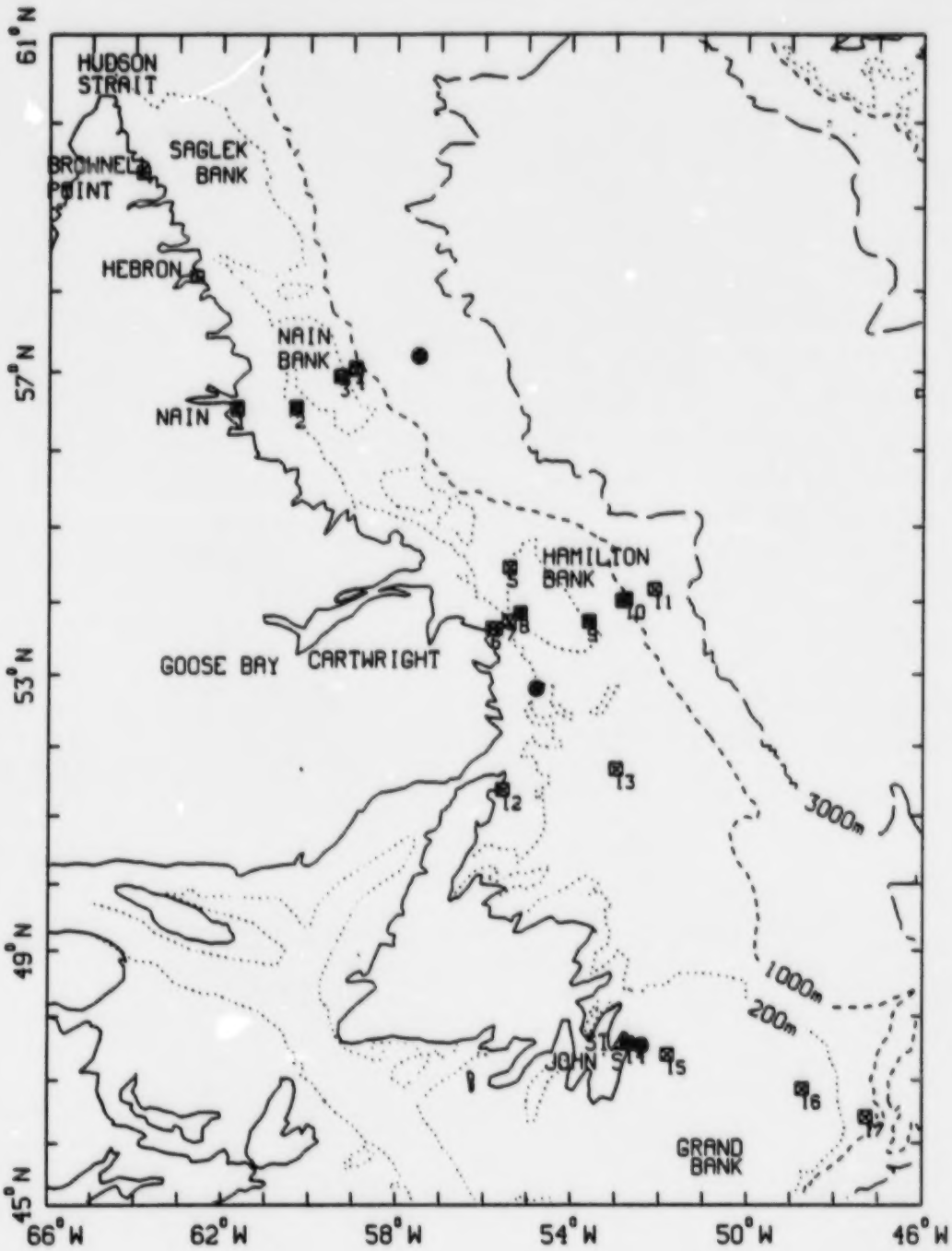

Figure 1. **The bathymetry of the Labrador/Newfoundland Shelf. Bottom pressure gauge sites are indicated by the boxed crosses and ECMWF wind sites are indicated by solid dots.**

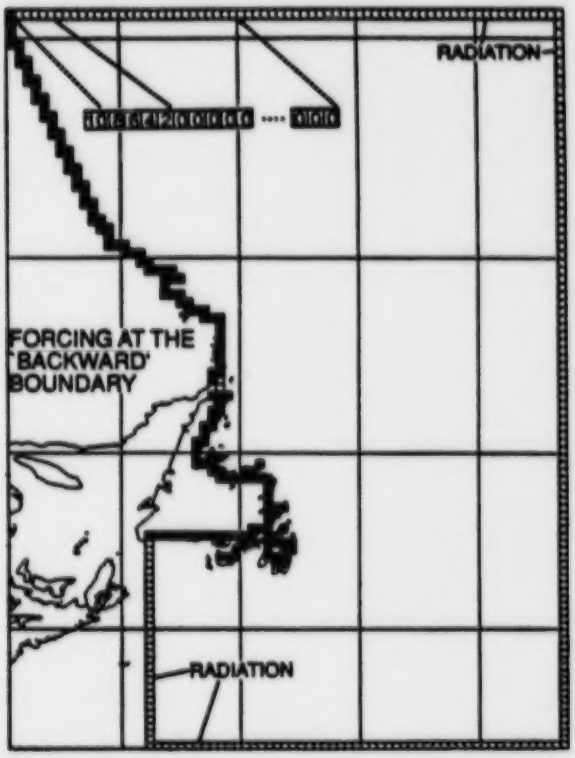

Figure 2. The open boundary conditions. Along the western side of the northern boundary, the amplitude of the sea level variations decreased linearly from 10 cm at the coast to 0 cm at the sixth offshore cell, and was held at zero for the cells indicated. Along the remaining part of the northern boundary, and along the other three parts of the open boundary, a radiation boundary condition was specified (see Appendix).

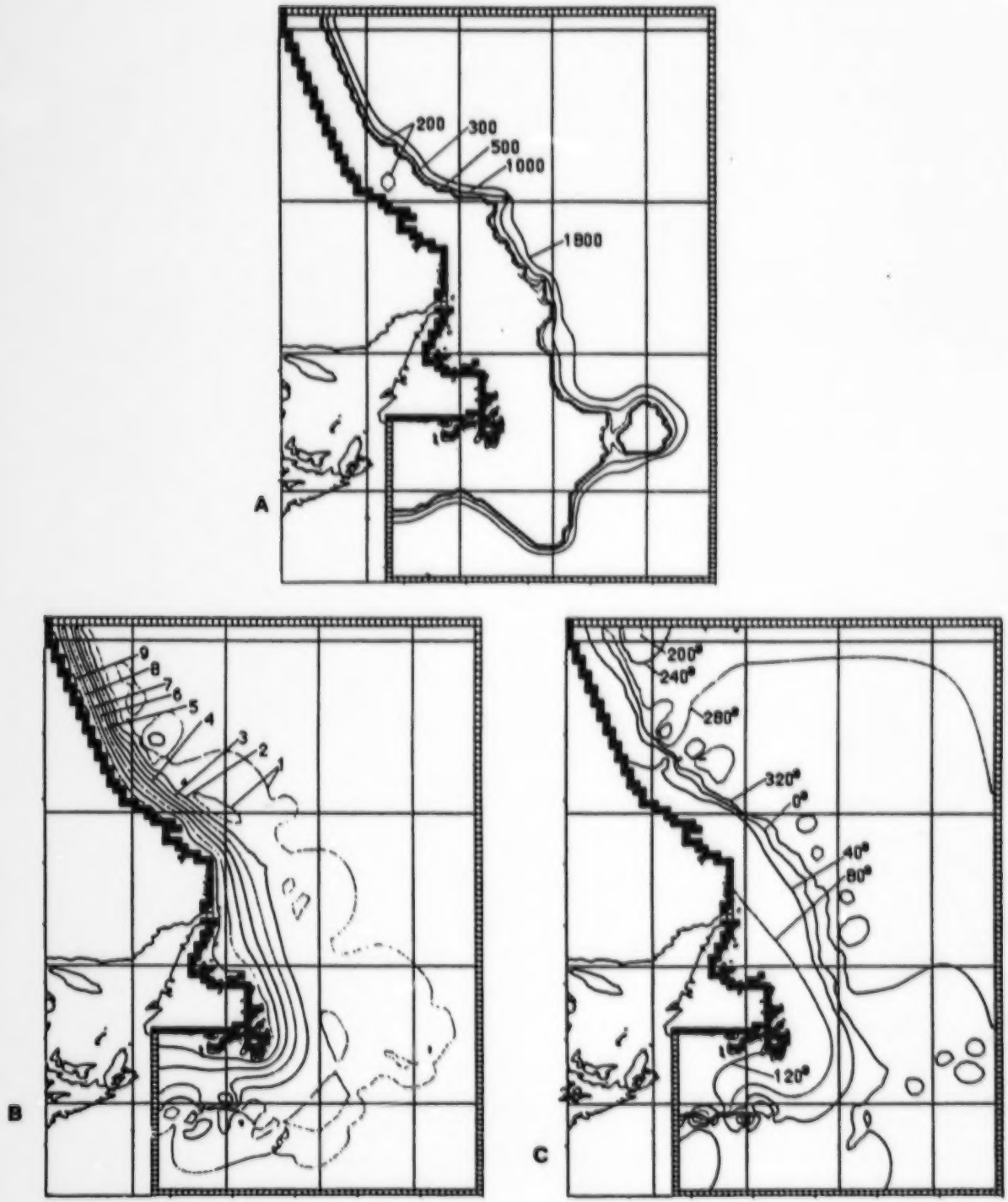

Figure 3. Model predictions for wave propagation down the Labrador Shelf. The model has been forced at the northern boundary by sea level variations with the cross-shelf structure shown in Figure 2, and a period of four days. Panels (b) and (c) correspond to the heavily-smoothed topography shown in (a), while (e) and (f) correspond to the more realistic topography shown in (d).

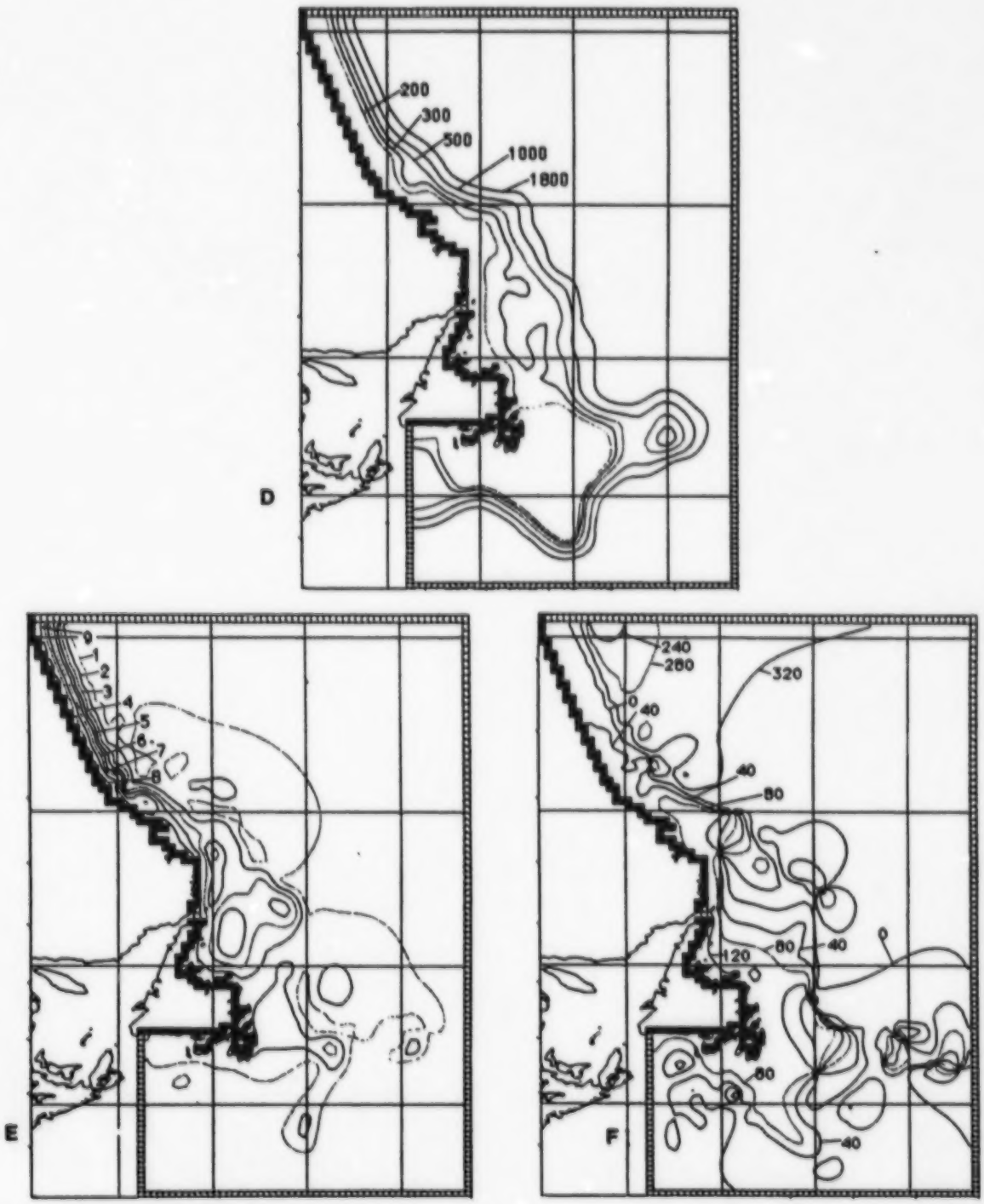

Figure 3. Continued.

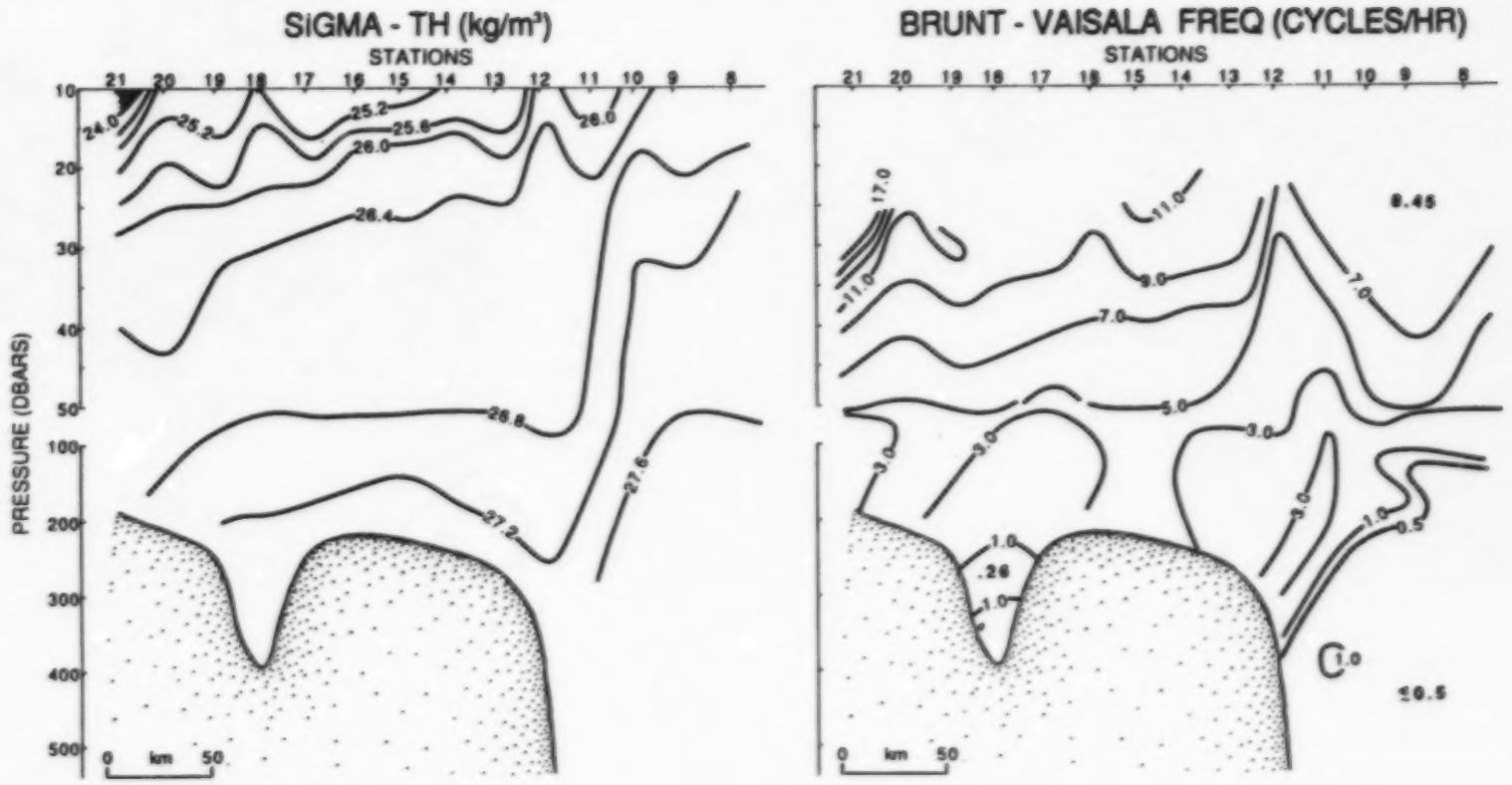

Figure 4. Density and buoyancy sections across Hamilton Bank determined from data collected during August, 1986.

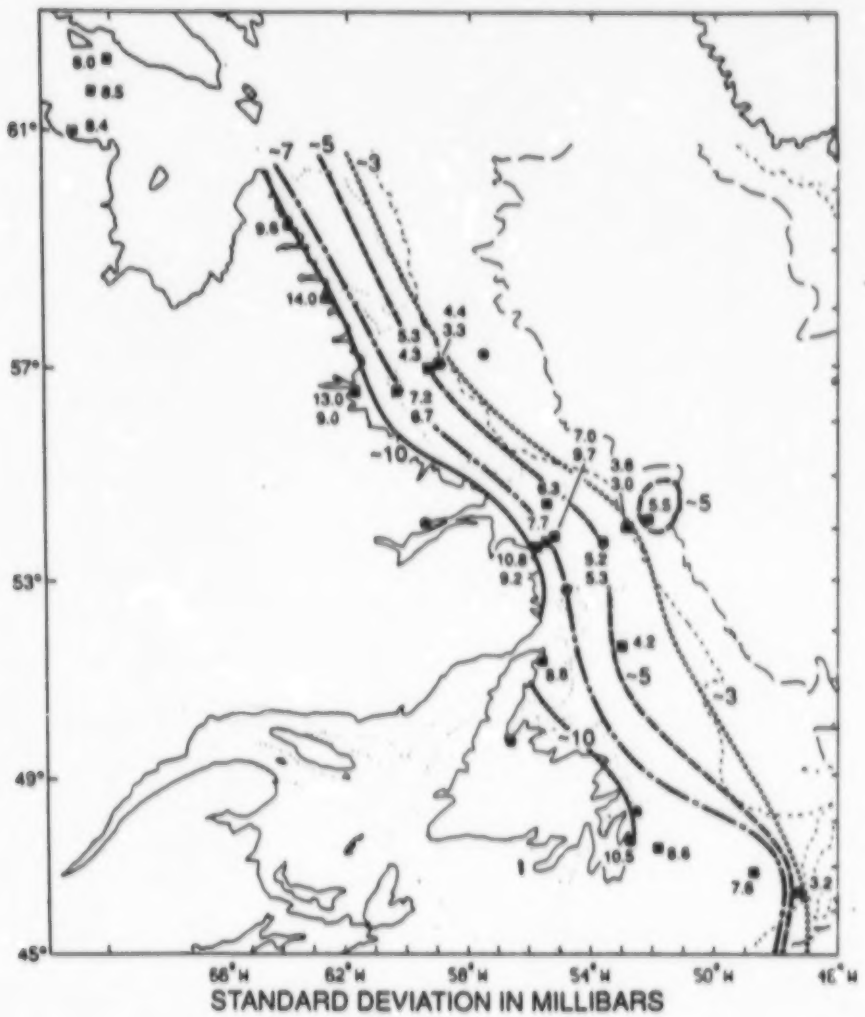

Figure 5. Root-mean-square pressure variations over the Labrador/Newfoundland Shelf. All data collected between 1985 and 1987 are shown. Where two numbers are associated with one point, they correspond to two distinct time intervals.

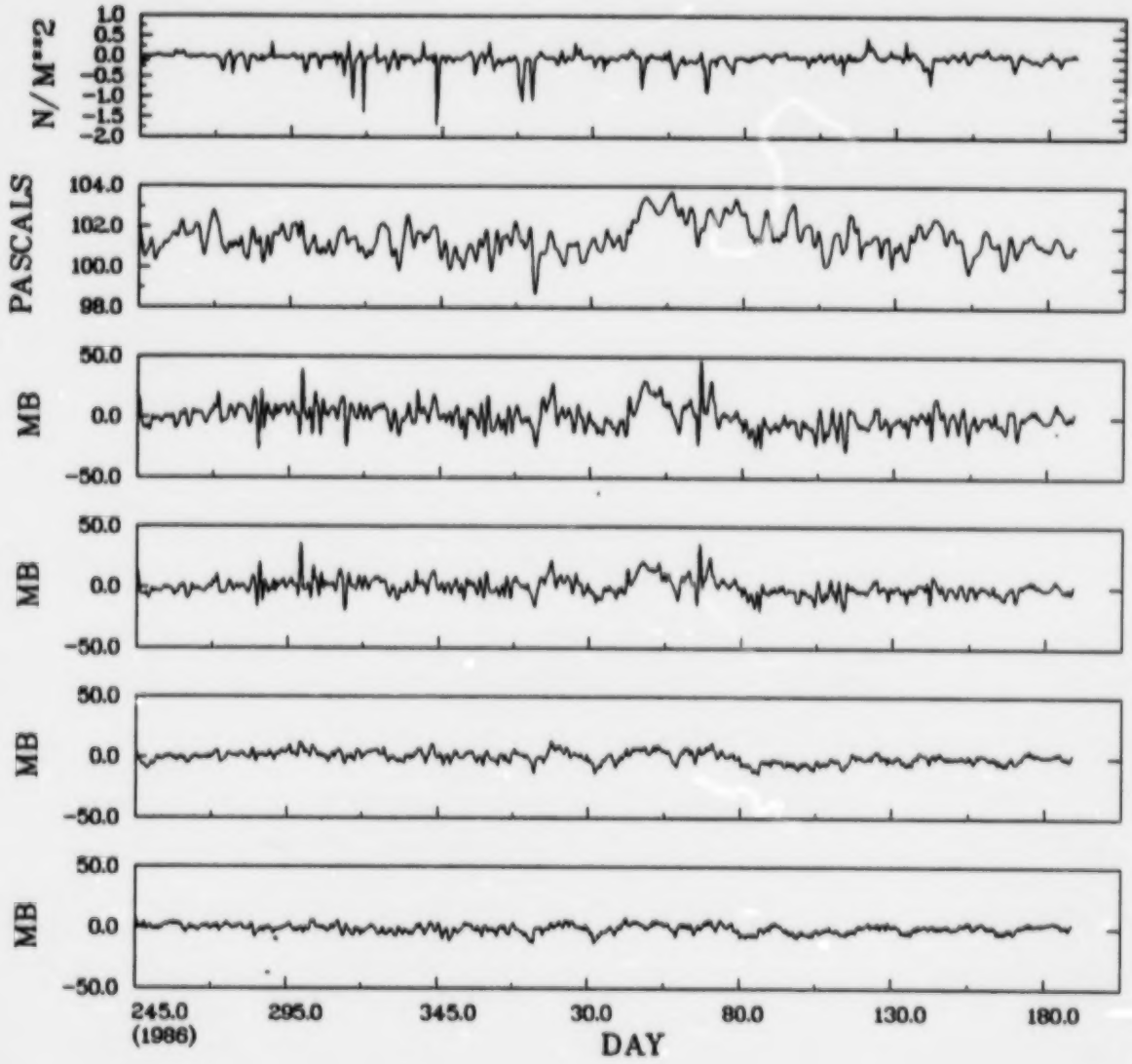

Figure 6. Time series of bottom pressure at the four sites across Nain Bank (sites 1-4). Distance seaward increases from top to bottom. The data have been de-tided and a low-pass filter has been applied which passes essentially all of the energy at periods exceeding 2 days and less than 2% of the energy at periods less than 1 day (see Wright, *et al.*, 1988 for details). The top two panels show the windstress corresponding to the central ECMWF site on Figure 1 and the average sea level pressure over Hudson Bay. Time is given in Julian days.

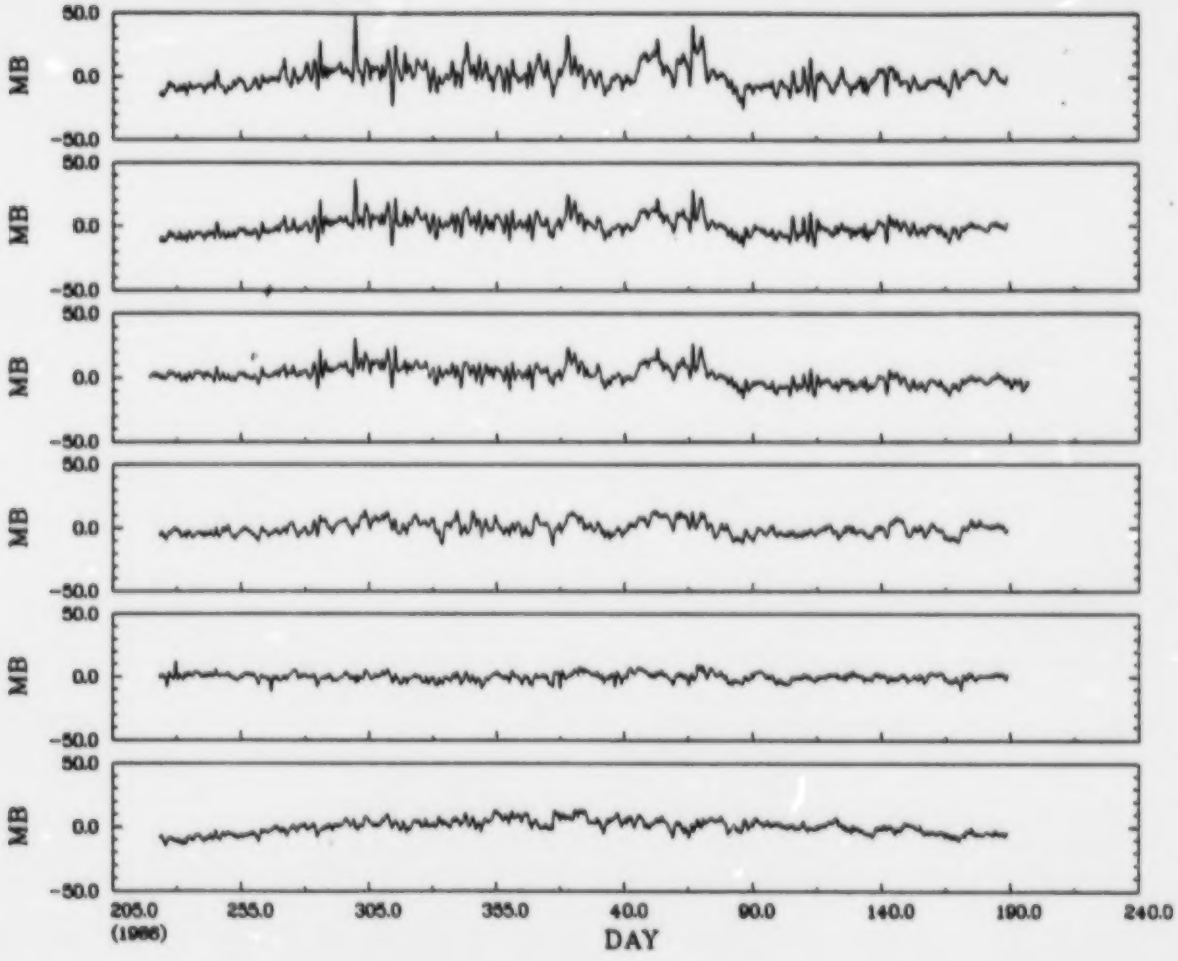

Figure 7. As in Figure 6 but for sites 6-11 across Hamilton Bank.

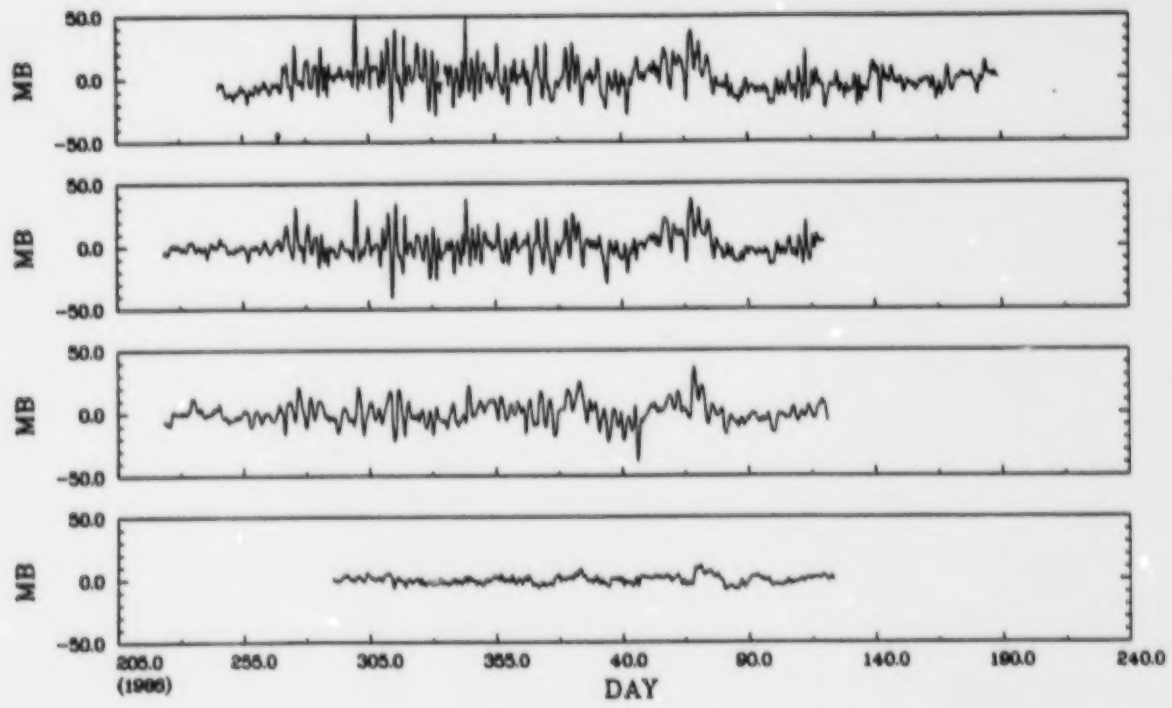

Figure 8. As in Figure 6 but for sites 14-17 across Grand Bank.

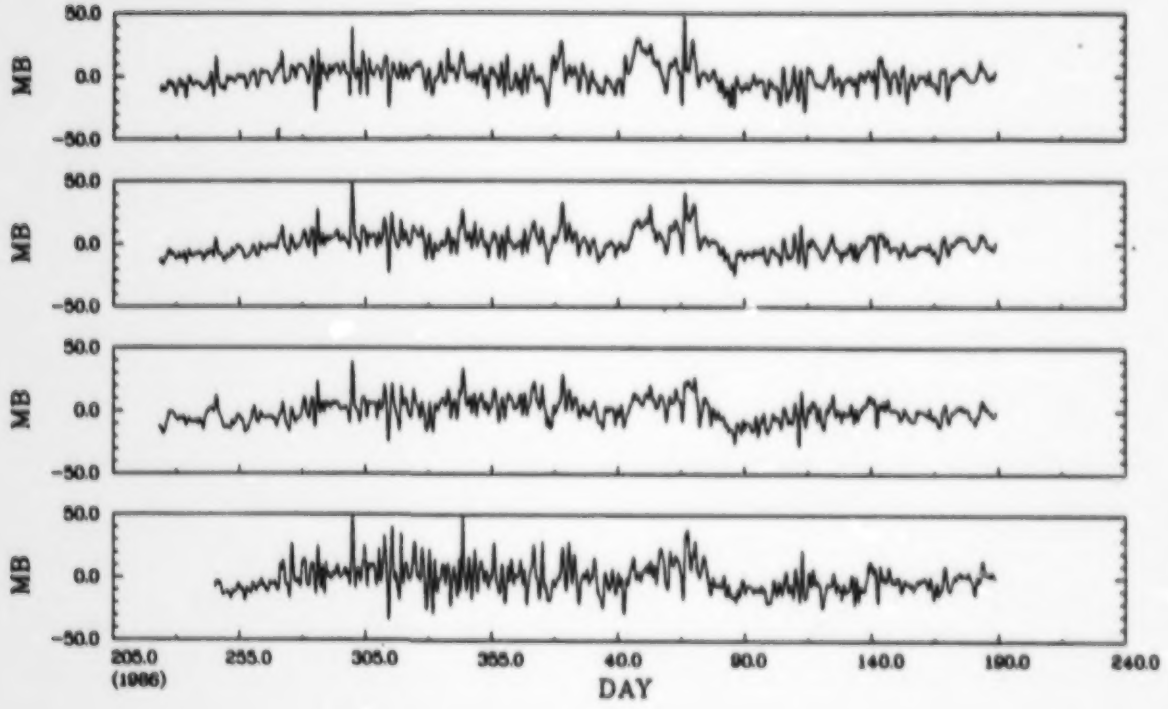

Figure 9. Time series of bottom pressure at the four coastal gauges (sites 1, 6, 12, 14). Distance south increases from top to bottom. Data were de-tided and filtered as described for Figure 6.

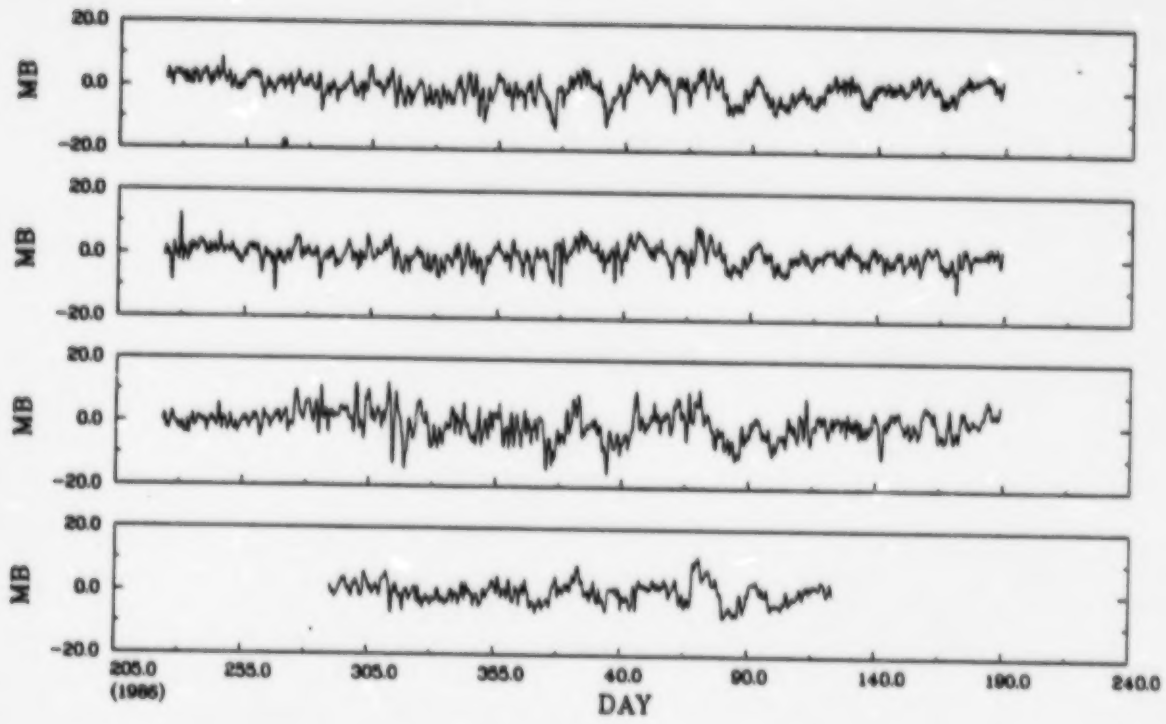

Figure 10. As in Figure 9 but for the four "shelf-break" gauges (sites 4, 10, 13, 17).

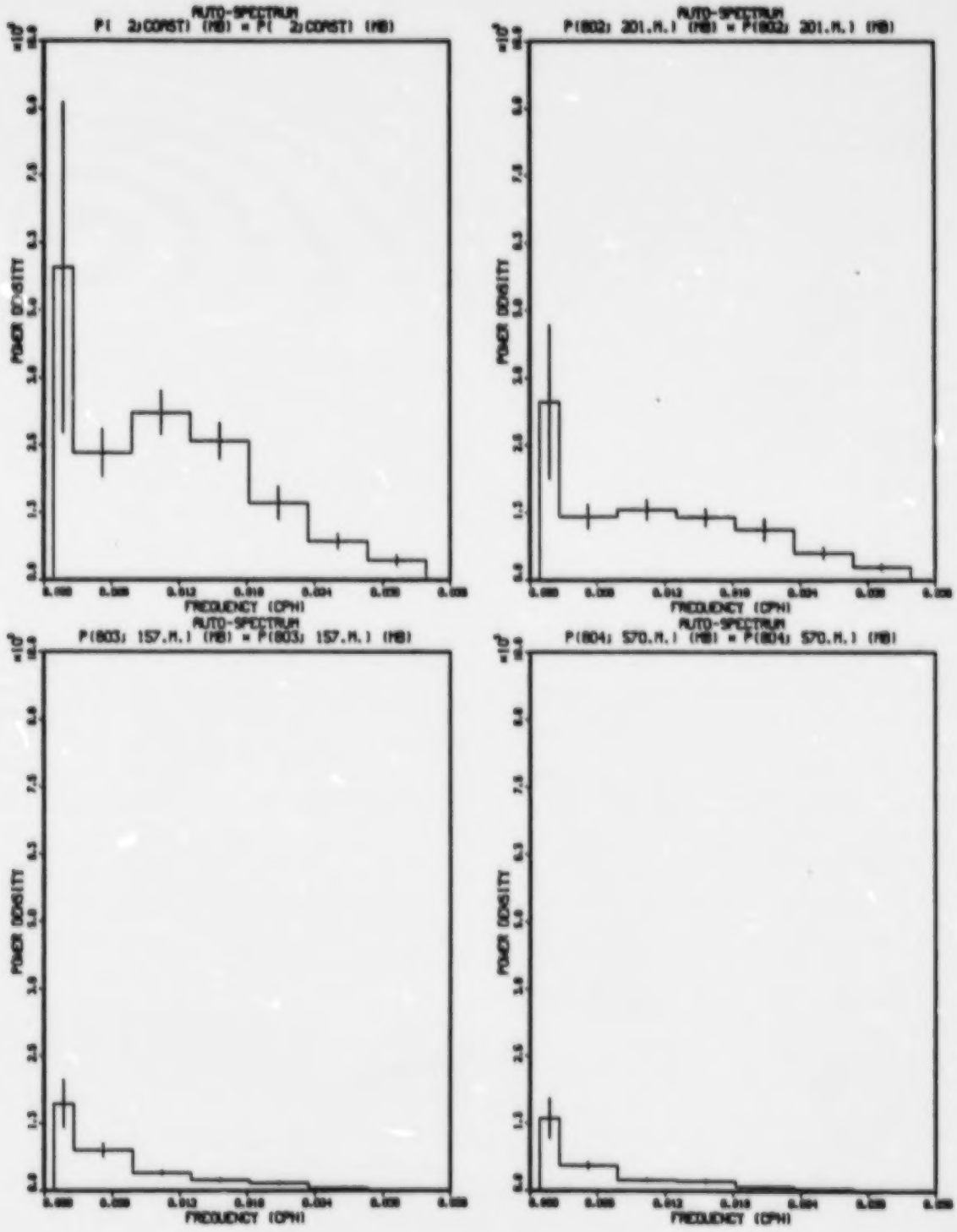

Figure 11. Power spectra corresponding to the records shown in Figure 6 (Nain Bank).

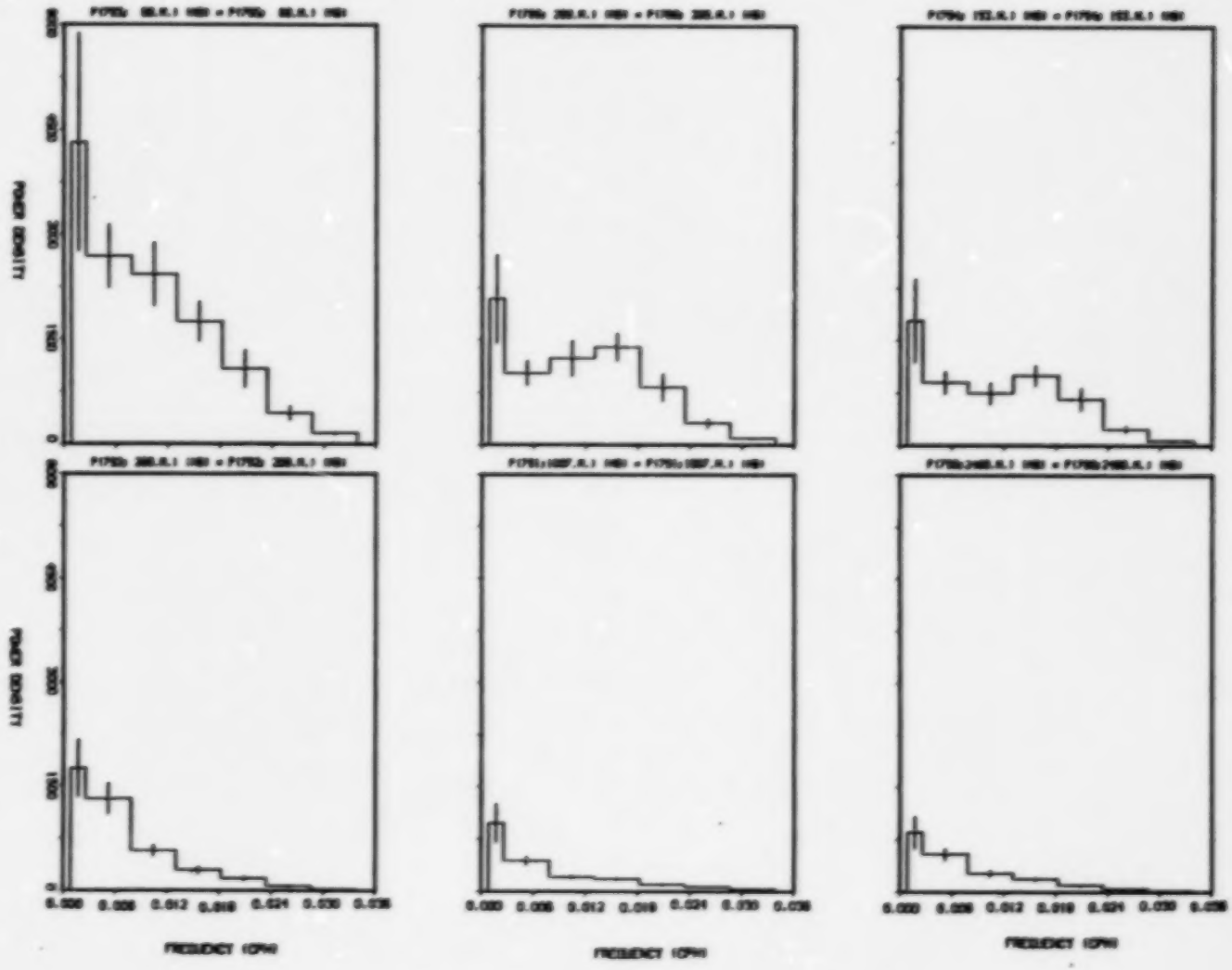

Figure 12. Power spectra corresponding to the records shown in Figure 7 (Hamilton Bank).

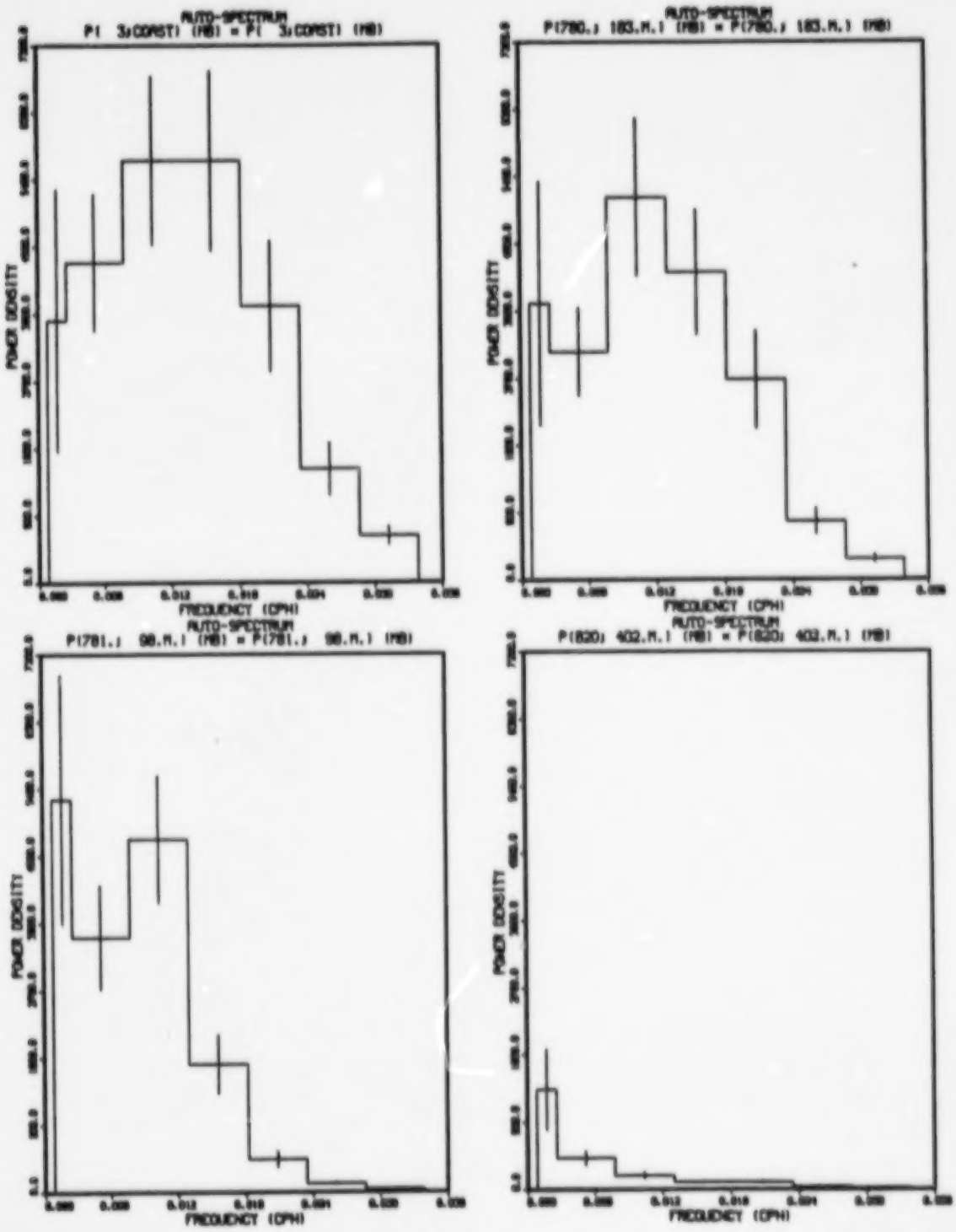

Figure 13. Power spectra corresponding to the records shown in Figure 8 (Grand Bank).

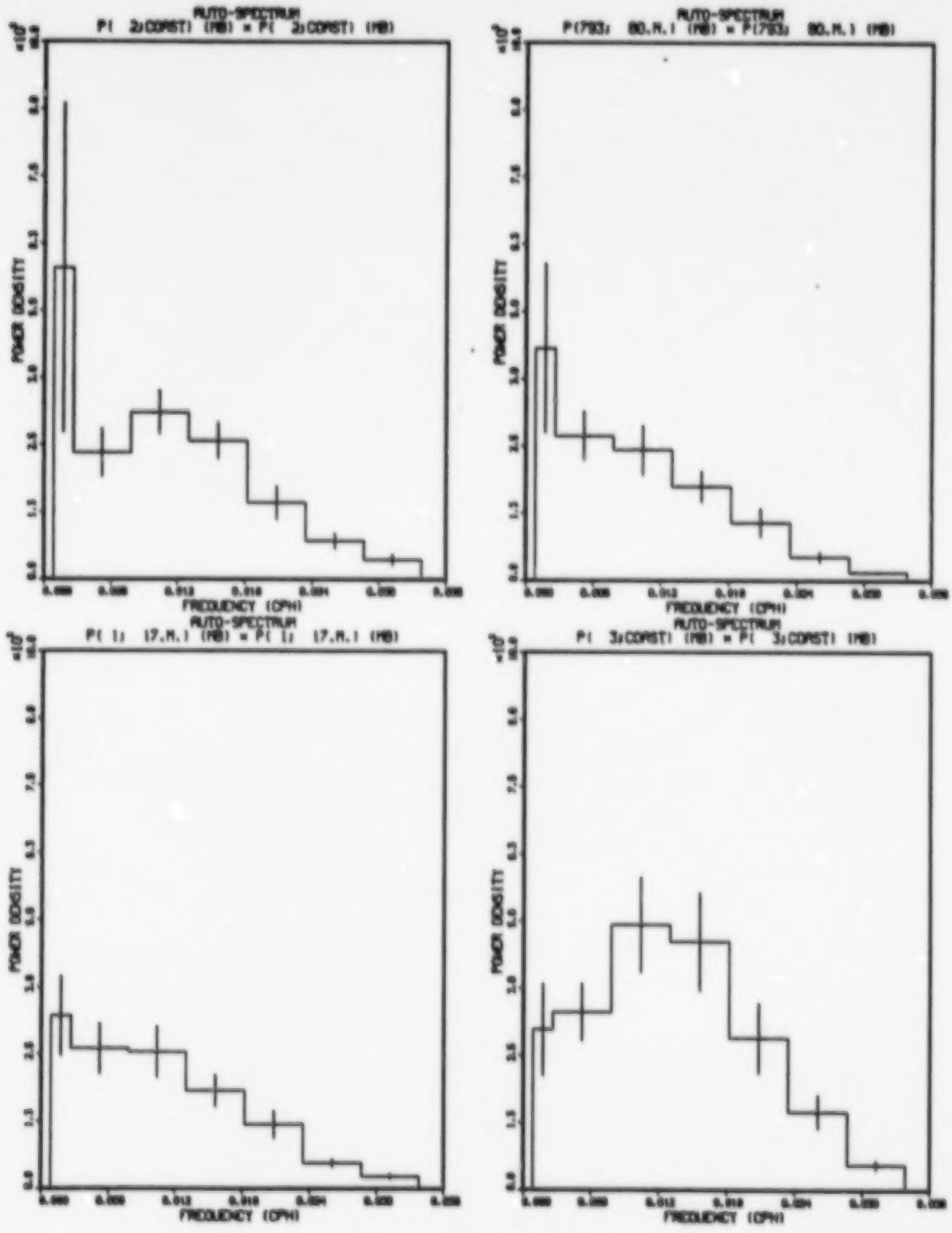

Figure 14. Power spectra corresponding to the records shown in Figure 9 (Coastal).

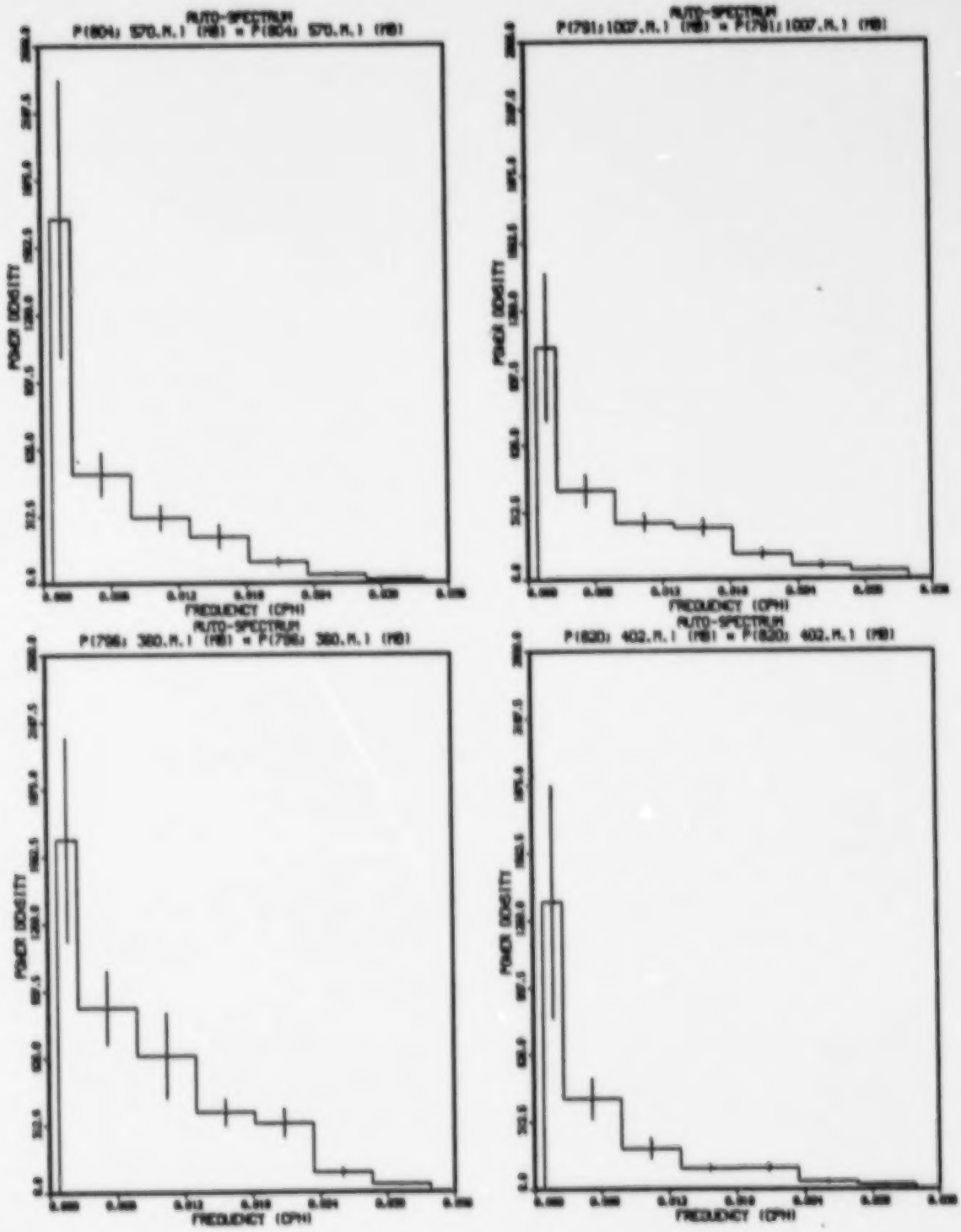

Figure 15. Power spectra corresponding to the records shown in Figure 10 (shelf-break).

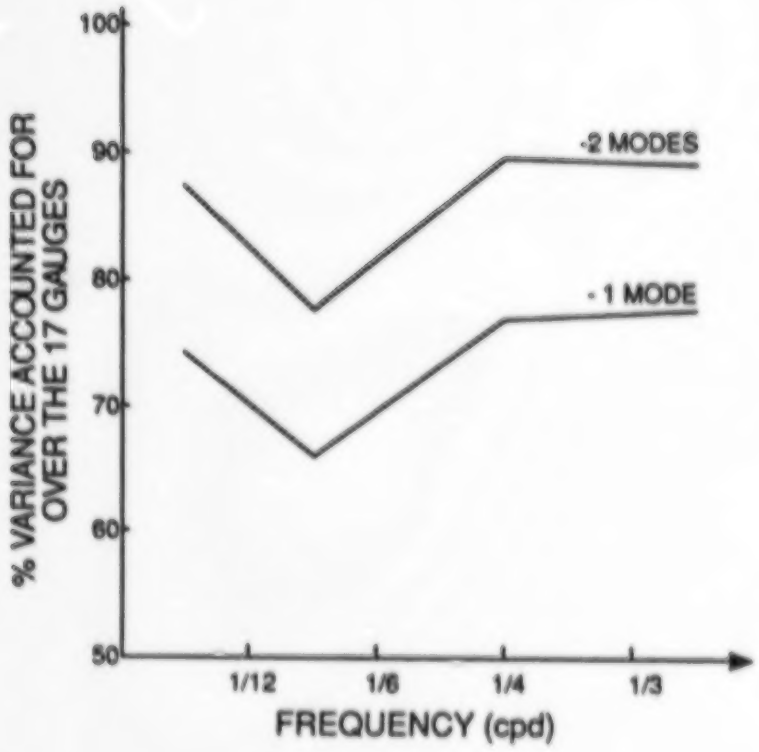

Figure 16. The percentage of energy over the 17 pressure records accounted for by the first two complex empirical orthogonal functions.

T= 24 d;
% variance = 74
DOF = 46(58)

Amplitude								Phase						
4.0(1)		3.3(2)		2.4(3)	1.8(4)			0		7		19	23	
			2.9(5)								18			
4.0(6)	3.0(7)	2.0(8)						14	14	16				
				1.9(9)	1.4(10)	1.1(11)						25	26	28
3.1(12)			1.9(13)					17			28			
3.0(14)	3.1(15)			2.2(16)	1.4(17)			28	25			29	26	

Figure 17. Amplitude and phase of the complex EOF for the frequency band centered on the 24 day period. The bracketed numbers in the amplitude panels correspond to the pressure gauges shown in Figure 1. Cross-spectral estimates used to determine the complex EOF have approximately 10 degrees of freedom.

T= 8 d;
% variance = 66
DOF = 45(30)

Amplitude								Phase						
4.6		3.5		2.3	1.0			0		6		29	13	
			2.6								27			
5.6	3.1	2.8						28	28	41				
				1.4	0.6	0.7						59	14	-25
5.4			1.8					38			32			
5.8	4.8			4.3	0.6			41	45			77	67	

Figure 18. As in Figure 17 but for the frequency band centered on a period of 8 days. Cross-spectral estimates have approximately 58 degrees of freedom.

T= 4.6;
% variance = 77
CEOF
Amplitude

Phase

4.7		2.4		1.7	1.3			0		-8		3	-16	
			3.1								22			
5.5	3.6	2.6						23	0	-6				
				1.7	1.0	1.2						-27	-18	-36
6.6			1.8					40			59			
7.3	7.0			5.5	0.6			41	53			124	47	

Figure 19. As in Figure 18 but for the frequency band centered on a period of 4 days.

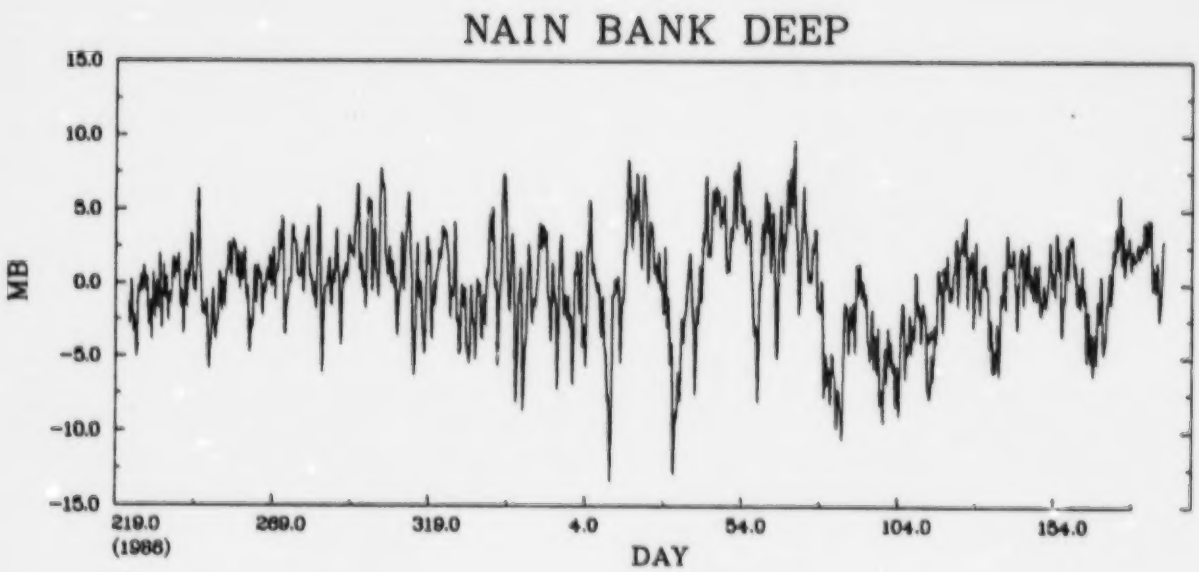

Figure 20. The average of the records from the two deepest pressure gauges on Nain Bank. This record is taken as a measure of the "offshore influence" in our regression models.

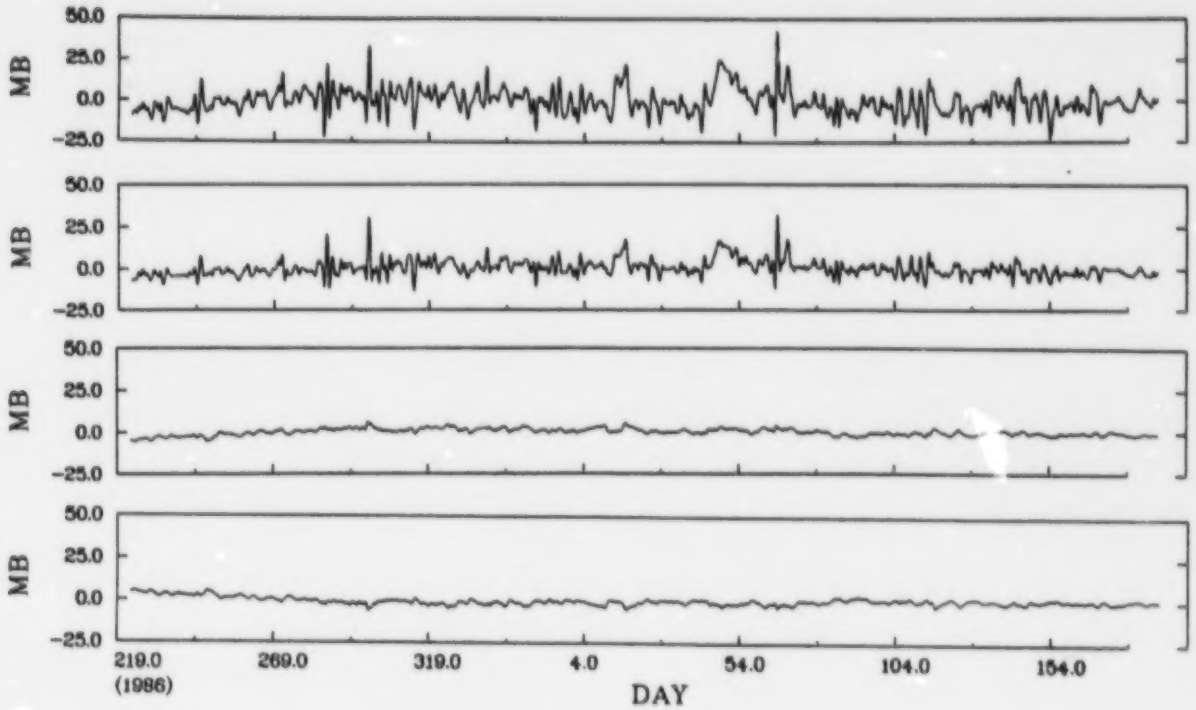

Figure 21. The residual pressure records for Nain Bank obtained by subtracting the signal shown in Figure 20 from each of the records shown in Figure 6. These records are taken to represent the coastally trapped wave signal propagating along the shelf.

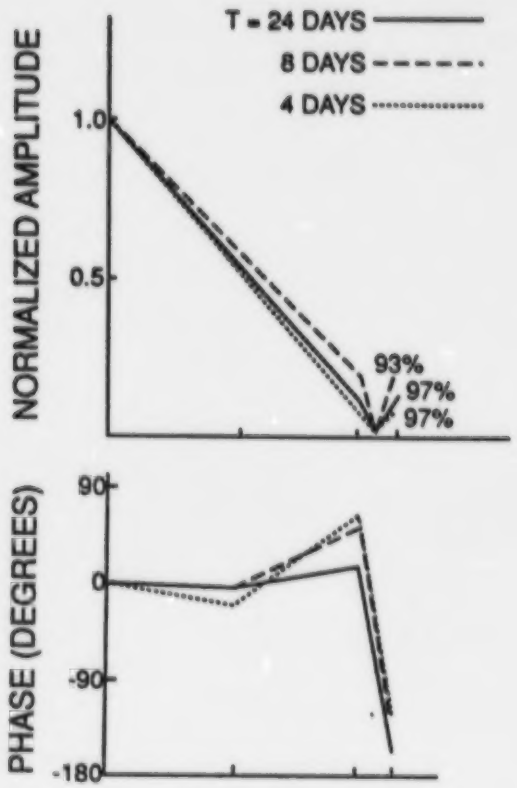

Figure 22. Normalized amplitudes and phases of the first complex EOF based on the four residual time series shown in Figure 24. Results are shown for the three primary frequency bands. Positive phase indicates a lag behind the coastal site. The percentages of residual variance accounted for by this one more are indicated in the upper figure. Tick marks on the horizontal axis indicate the measurement locations. The distance from the inner to the outer mooring is approximately 160 km.

M1: Period = 24 d

Amplitude								Phase						
.88(.04)		.46(.06)		.11(.07)	.11	(.07)		-.5(2)		1(8)		18(40)	-162(40)	
			.33(.15)								22(28)			
.54(.18)	.27(.12)	.28(.17)						18(20)	23(25)	28(37)				
				.07(.28)	.10(.15)	.13(.18)						-4(180)	-80(180)	104(180)
.27(.25)			.08(.22)					38(180)			-149(180)			
.23(.4)	.4(.4)			.3(.6)	.1(.4)			117(180)	123(180)			116(48)	152(180)	

Figure 23. Amplitude and phase of the response to the coastally trapped wave signal for the frequency band centered on a period of 24 days. Bracketed quantities correspond to the 90% confidence interval . Degrees of freedom ~15 for sites 1-13 and ~10 for sites 14-17.

T= 8; M1
DOF = 45(30)
Amplitude

Phase

.86(.03)		.47(.06)		.14(.05)	.14(.05)			-.2(2)		-2(6)		58(20)	-121(20)	
			.37(.1)								21(21)			
.50(.1)	.16(.1)	.15(.1)						29(15)	17(49)	55(63)				
				.18(.2)	.12(.1)	.19(.1)						118(180)	-94(65)	-90(42)
.27(.2)			.09(.2)					30(44)			-75(180)			
.13(.3)	.2(.3)			.4(.4)	.08(.1)			90(180)	106(180)			103(76)	-67(180)	

Figure 24. As in Figure 23 but for the frequency band centered on a period of 8 days. Degrees of freedom 45 for sites 1-13 and ~30 for sites 14-17.

T= 4; M1
DOF = 15(10)
Amplitude

Phase

.89(.02)		.46(.04)		.06(.03)	.06(.03)			.2(2)		-21(5)		81(39)	-99(39)	
			.24(.11)								-2(28)			
.23(.1)	.23(.1)	.18(.09)						24(30)	-19(26)	-37(30)				
				.05(.1)	.08(.06)	.09(.03)						-61(180)	-87(50)	-123(67)
.09(.1)			.06(.1)					47(180)			-48(180)			
.13(.28)	.03(.29)			.12(.42)	.09(.09)			103(180)	46(180)			-21(180)	-49(180)	

Figure 25. As in Figure 23 but for the frequency band centered on a period of 4 days. Degrees of freedom 45 for sites 1-13 and ~30 for sites 14-17.

T= 24; M2
DOF = 15(10)
Amplitude

Phase

.96(.06)		1.1(.11)		1.0(.12)	.99(.12)			.9(4)		-.9(6)		-1(7)	1(7)	
			.90(.27)								7(17)			
1.0(.32)	.91(.20)	.79(.29)						0(18)	.6(13)	2.7(21)				
				.82(.48)	.71(.25)	.80(.31)						16(38)	14(21)	-22(31)
.96(.51)			.88(.38)					-1(32)			9(26)			
.88(.67)	.95(.65)			.78(.92)	.44(.60)			-17(50)	-21(44)			-21(180)	-16(180)	

Figure 26. As in Figure 23 but for the "offshore influence".

T= 8; M2
DOF = 45(30)

Amplitude								Phase						
.97(.07)		1.0(.1)		1.1(.1)	.94(.1)			2(4)		-1(6)		0(5)	0(6)	
			.95(.3)								4(17)			
1.1(.3)	.95(.3)	.86(.1)						0(15)	0(11)	5(18)				
				.71(.5)	.69(.2)	.66(.3)						11(42)	6(18)	-9(23)
.80(.4)			.75(.3)					2(29)			14(26)			
.78(.58)	.67(.62)			.85(.50)	.47(.33)			18(49)	18(68)			11(69)	1(44)	

Figure27. As in Figure 24 but for the "offshore influence".

T= 4; M2
DOF = 45(30)

Amplitude								Phase						
.96(.09)		1.1(.16)		1.1(.13)	.94(.13)			3(5)		-5(8)		1(7)	-1(8)	
			.97(.41)								7(25)			
1.3(.44)	1.0(.37)	1.0(.34)						0(20)	-2(21)	3(19)				
				1.0(.45)	0.9(.23)	0.9(.29)						9(26)	11(15)	-13(20)
1.1(.58)			0.7(.51)					15(31)			7(49)			
.68(.83)	.86(.84)			.35(1.2)	.57(2.6)			32(180)	35(76)			68(180)	15(27)	

Figure 28. As in Figure 25 but for the "offshore influence".

T= 24; v^2
DOF = 15(10)
Amplitude

Phase

3.2(4.9)		6.0(8.4)		3.6(9.5)	3.6(9.5)			-66(180)		0(180)		-86(180)	94(180)	
			4.1(21.0)								21(180)			
14.7(25.1)	9.8(15.3)	7.9(22.6)						7(180)	30(180)	13(180)				
				13.0(38)	6.2(19.9)	20.3(24.5)						162(180)	77(180)	180(180)
14.0(40)			8.6(30)					60(180)			125(180)			
28(62)	32(61)			42(85)	30(55)			79(180)	82(180)			15(180)	79(180)	

Figure 29. As in Figure 23 but for the cross-shelf stress component.

T = 8; τ^2
DOF = 45(30)

Amplitude

5.9(3)		7.6(4)		1.7(4)	1.7(4)		
			14.6(12)				
21.4(12)	12.8(11)	9.7(12)					
				2.0(20)	5.3(9)	8.3(11)	
17.2(17)			2.6(14)				
17(25)	11(27)			28(34)	.6(14)		

Phase

148(23)		-31(35)		2(180)	-178(180)	
			16(54)			
12(34)	25(58)	28(180)				
				173(180)	176(180)	-172(180)
80(79)			96(180)			
127(180)	66(180)			10(180)	-58(180)	

Figure 30. As in Figure 24 but for the cross-shelf stress component.

T= 4; v^n
DOF = 45(90)
Amplitude

Phase

.98(2.4)		1.3(4.3)		2.2(3.6)	2.2(3.6)			-179(180)		-25(180)		107(180)	-73(180)	
			6.2(11)								88(180)			
17.6(12)	9.4(10)	2.7(9)						55(43)	40(180)	52(180)				
				6.6(12)	1.3(6)	2.3(8)						-168(180)	-107(180)	-116(180)
27(16)			14(14)					81(37)			93(86)			
29(28)	27(26)			35(34)	5(8)			86(180)	74)			124(180)	47(180)	

Figure 31. As in Figure 25 but for the cross-shelf stress component.

T = 24; σ
DOF = 15(10)
Amplitude

Phase

1.0(4)		.82(6)		3.0(7)	3.0(7)			94(180)		-63(180)		-89(180)	91(180)	
			12.3(16)								-148(180)			
22(19)	8.7(12)	8.4(17)						-151(61)	-132(180)	-103(180)				
				10(29)	5.4(15)	2.1(19)						-108(180)	4(180)	98(180)
23(30)			7(23)					173(180)			100(180)			
45(42)	30(41)			19(58)	9.8(37)			167(70)	176(180)			-4(180)	16(180)	

Figure22. As in Figure 23 but for the along-shelf ('northward') stress component.

T = 8; σ
DOF = 45(30)
Amplitude

Phase

1(3)		1.9(3)		2.6(3)	2.6(3)			-4(180)		-130(180)		164(180)	-16(180)	
			9.8(.8)								-133(54)			
22(8)	10(7)	8.6(8)						-158(21)	-154(44)	-126(81)				
				7.6(13)	4.5(6)	1.4(7)						9(180)	-22(180)	-3(180)
33(11)			7.6(9)					-167(19)			163(180)			
53(16)	36(18)			24(22)	11(9)			-174(18)	-167(30)			-79(71)	-60(37)	

Figure 33. As in Figure 24 but for the along-shelf ('northward') stress component.

T= 4; ☞
DOF = 45(30)
Amplitude

Phase

1.8(1.6)		3.6(2.8)		1.5(2.3)	1.5(2.3)			35(62)		-161(50)		136(180)	-44(180)	
			11(7.3)								-150(41)			
26(7.8)	12(6.6)	5.6(6.1)						-163(17)	161(33)	146(180)				
				8.9(8.1)	3.8(4.1)	.5(5.3)						64(65)	3(180)	-145(180)
32(10.5)			11(9.1)					-156(19)			-114(55)			
59(18)	50(18)			49(26)	9(6)			-162(18)	-141(21)			-54(33)	-39(39)	

Figure 34. As in Figure 25 but for the along-shelf ('northward') stress component.